MB 2020-03

Timing of crustal deformation in Archean rocks along the northern boundary of the Opinaca and La Grande subprovinces, Eeyou Istchee Baie-James region, Québec Superior Province

Documents complémentaires

Additional Files

Licence

License

Énergie et Ressources naturelles
Québec

Timing of crustal deformation in Archean rocks along the northern boundary of the Opinaca and La Grande subprovinces, Eeyou Istchee Baie-James region, Québec Superior Province

Nathan R. Cleven, Carl Guilmette, Lyal B. Harris et Don W. Davis

MB 2020-03

Énergie et Ressources naturelles
Québec

Timing of crustal deformation in Archean rocks along the northern boundary of the Opinaca and La Grande subprovinces, Eeyou Istchee Baie-James region, Québec Superior Province

Ministère de l'Énergie et des Ressources naturelles, Québec

by

Nathan R. Cleven[1], Carl Guilmette[1], Lyal B. Harris[2], Don W. Davis[3]

[1]Université Laval, Département de géologie et de génie géologique

[2]Institut National de la Recherche Scientifique (INRS)

[3]Jack Satterly Institute of Geochronology, University of Toronto

Abstract

This report provides a structural analysis of two areas in the Eeyou Istchee Baie James region of Québec, with U-Pb zircon and monazite geochronology applied to establish the timing of specific structures and regional deformation events. Megascopic shear-related fold structures in amphibolites of the western La Grande subprovince, in the Lac Sakami region along the Opinaca boundary, have associated north-dipping distributed shear zones that indicate ca. 2840 Ma rocks were thrust over ca. 2740 Ma Yasinski group volcanics in a ca. 2725-2710 Ma southward directed convergent event. Timing of thrusting is interpreted from weakly deformed dykes crosscutting mylonitic rocks. Shear zones and their north-over-south sense of motion are characterized with field observations, analysis of structural data, and microstructural analysis. Regional fold patterns in the Lac Joubert region straddling the boundary between the eastern La Grande and Opinaca indicate that a 6-8 km wide domain we label the Boisbriand exhibits structures resulting from bulk shortening, including pervasive tight to isoclinal overturned folds, associated with the La Grande overriding the Opinaca. Folds within the Opinaca have a similar shallowly east plunging orientation yet are more open. This episode of convergence is estimated to coincide with a metamorphic episode defined by multiple ca. 2652 Ma monazite ages, all within error. A second generation of open folds with a N-S orientated subhorizontal axis is superposed on shallowly east plunging folds of the La Grande, thus forming a dome and basin fold interference pattern at the map scale. This second folding event did not affect the Boisbriand or the Opinaca to the south, thus the Pradier shear zone acted as a detachment to permit the E-W shortening. This episode of deformation may be associated with a second pulse of monazite crystallization ca. 2636 Ma. Dextral shearing along the Pradier and Orillat shear zones, which bound the Boisbriand, is interpreted to have waned by 2625 Ma from the age of a pegmatite in a parallel shear zone further north. These results indicate that the northern boundary region between the La Grande and the Opinaca subprovinces developed through multiple deformation and metamorphic events that spanned over 100 m.y., from ca. 2725-2610 Ma.

Ce rapport présente une analyse structurale détaillée de deux secteurs de la région de Eeyou Istchee Bay James au Québec. Ces travaux s'appuient sur des datations U-Pb de zircons et de monazites qui ont permis d'établir l'âge des structures et des évènements de déformation régionaux. Des plis mégascopiques liés au cisaillement dans les amphibolites de la partie ouest de la Sous-province de La Grande, dans la région du lac Sakami, au contact de la Sous-province d'Opinaca, sont associés à des zones de cisaillement à pendage vers le nord. Cette observation indique que les roches gneissiques du Complexe de Langelier (~2840 Ma) ont été chevauchées vers le sud sur les volcanites de la Formation de Yasinski (~2740 Ma) lors d'un évènement de convergence vers 2725-2710 Ma. La chronologie du chevauchement a été interprétée en datant les dykes faiblement déformés qui coupent les zones de mylonite Les caractéristiques des zones de cisaillement et leur mouvement du nord vers le sud ont été établis à partir des observations de terrain, de l'étude des données structurales et de l'analyse microstructurale.

Dans la région du lac Joubert, à la limite du La Grande et l'Opinaca, un domaine de 6 à 8 km de large désigné comme le domaine de Boisbriand, présente des structures caractéristiques d'un raccourcissement global, incluant des plis renversés serrés à isoclinaux attribuables au chevauchement du La Grande sur l'Opinaca. Les plis dans l'Opinaca présentent un faible plongement vers l'est, mais sont plus ouverts. Cet épisode de convergence semble correspondre à un évènement métamorphique défini par plusieurs âges sur monazites autour de 2652 Ma. Une seconde génération de plis ouverts N-S d'axe subhorizontal se superpose à la première génération de plis à faible plongement vers l'est, formant ainsi un motif d'interférence en dômes et bassins à l'échelle de la carte. Ce second évènement de plissement n'a pas affecté le Boisbriand ou l'Opinaca au sud, la Zone de cisaillement Pradier ayant agi comme une zone de détachement qui a permis d'accommoder le raccourcissement E-W. Cette phase de déformation serait associée à un second épisode de cristallisation de la monazite à ~2636 Ma. Le mouvement dextre le long des zones de cisaillement de Pradier et d'Orillat, qui bordent le Boisbriand, se serait terminé vers 2625 Ma, comme l'indique l'âge d'une pegmatite qui coupe une zone de cisaillement parallèle plus au nord. Ces résultats démontrent que la limite nord entre le La Grande et l'Opinaca s'est développée au cours de multiples épisodes de déformation et de métamorphisme entre 2725 et 2610 Ma.

Table of contents

List of Figures

List of Tables

1. Introduction

1.1 Problematic

The boundary between the La Grande and Opinaca subprovinces of the northeast Archean Superior Province in Québec is a significant crustal structure that separates two vastly different lithotectonic assemblages of different ages. However, it is not yet understood how or when the structure originally formed, such as if it is associated with the formation of the Opinaca basin, or events prior, or if it developed during later tectonism. The examination of old structures is restricted to analysis of the La Grande, as it hosts Paleo- to Mesoarchean rocks, yet much of its extent was defined in the early Neoarchean. Regional time constraints on deformation within the La Grande are restricted to ca. 2720-2705 Ma widespread plutonism that constrains subsequent formation of tight synclinal fold structures in greenstone belts which wrap around intrusions, and late- to post-tectonic (ca. 2625-2610 Ma) pegmatite dykes that intruded the boundary zone. It is unclear whether or not linear east-west oriented faults that traverse the subprovince are related to earlier phases of deformation. High-grade metasedimentary and metaplutonic rocks in the East of the La Grande also present unanswered questions as to whether they were created and deformed in a similar event, with similar characteristics, as the formation of the Opinaca. To adequately understand the metallogeny of mineral occurrences along the boundary requires the establishment and comparison of phases of convergent, divergent, or shear related deformation in each subprovince, and how the different subprovinces, with their extremely different rheologies, interacted along their interface.

1.2 Objectives

The goal of this report is to provide relative and absolute age constraints for structures that are representative of regional deformation phases in the Eeyou Istchee Baie-James region of the Northeast Superior Province, Québec. Field-based structural analysis permits characterization of regional structures, which in turn establishes context for U-Pb zircon and monazite ages from samples targeted to constrain deformation. Two study regions along the West and East portions of the La Grande-Opinaca boundary were selected as each exhibits structures associated with different phases of deformation. In the western map area, the Lac Sakami region, structures within an amphibolite-grade greenstone belt were targeted for analysis of early, east-west oriented structures within the La Grande. The objective for geochronology within this region is to provide specific ages of metamorphic protoliths, and constraints on ages of their respective deformation through dating igneous units deformed during different phases of shearing and folding. In the eastern map area, the Lac Joubert region, regional structures in orthogneiss and paragneiss are examined to characterize and compare phases of convergence between the La Grande and Opinaca, as well as late phases of shearing and east-west shortening. The objective of U-Pb monazite geochronology within this region is to provide the timing of phases of peak metamorphism, which may be either episodes of high-temperature, low-pressure metamorphism, or convergence and crustal thickening, but in turn may be a likely proxy for the timing of folding. Map-scale analysis of large structures is essential to analyze the high-grade nature of the regional deformation events. We expect that the drastic rheological differences between the two regions may provide insight on uneven strain distributions and strain partitioning along the deformed La Grande-Opinaca boundary region. A comprehensive view of the style of crustal deformation of Archean rocks within the Eeyou Istchee Baie-James region is presented.

1.3 Project location

The study area are located in two different sectors of the La Grande subprovince, where in immediate contact with the Opinaca subprovince. These are in the geographic region of the Eeyou Istchee Baie-James, Québec. The first sector, in the West, is located Northeast of Lac Sakami and Southeast of the Robert Bourassa reservoir. The map area is relatively small, a 3 by 6 km section of map sheet SNRC 33F09 (Figure 1B). The second study region, in the East, located near Lac Joubert, encompasses three map sheets, SNRC 33H01, 23E04, and 23E03 (Figure 1B).

1.4 Geologic context

The Eeyou Istchee Baie-James region of northern Québec is geologically comprised of gneissic-plutonic, volcano-plutonic, and metasedimentary domains of the Archean Northeastern Superior Province (Figure 1A). It constitutes six subprovinces (from North to South): the Minto, the La Grande, the Opinaca, the Ashuanipi, the Nemiscau, and the Opatica (Ciesielski, 1991; Percival et al., 2012). The La Grande and Opinaca subprovinces are the focus of this report. Within the region, Archean rocks are locally intruded by Proterozoic mafic dykes (Buchan et al., 2007), and are locally overlain by Proterozoic sediments, such as the Sakami basin.

1.4.1 The Opinaca subprovince

The Opinaca subprovince comprises high-grade metasedimentary rocks that host extensive syn- to post-tectonic intrusions. Geochronological constraints on deposition of Opinaca sediments are limited to intrusions within metasedimentary rocks, including the Marjoulet tonalitic gneiss (2689 ± 4 Ma; SIGÉOM 2018, data unpublished) and the Féron suite tonalite (2710 ± 2 Ma; Augland et al., 2016). Metasedimentary protoliths have been interpreted to be wacke with a minor constituent of pelite. Rare conglomeratic horizons, stratiform iron formations, tuffs, and amphibolites outcrop in proximity to its boundary with the La Grande (Bandyayera et al., 2010). Neither the underlying basement nor the original geodynamic setting that formed the basin has yet to be determined.

The majority of the central to eastern Opinaca subprovince was subjected to a peak of granulite grade metmorphism. An early metamorphic stage that occurred prior to deformation was likely high-temperature, low-pressure (Cadéron, 2003; Côté-Roberge, 2018), a characteristic noted within other metasedimentary subprovinces (Harris and Goodwin, 1976; Kehlenbeck, 1976; Percival, 1989; Piette-Lauzière et al., 2019). Migmatization of the metasediments in these regions ca. 2665-2635 Ma was contemporaneous with injections of leucocratic melt sourced from below (Morfin et al., 2013; Côté-Roberge, 2018). Significant volumes of this anatectic melt accumulated at and percolated through the currently exposed structural level, forming an “injection complex” (Morfin et al., 2013). Stromatic layering in migmatites (Bandyayera et al., 2010; Côté-Roberge et al., 2016) was folded during a phase of widespread, penetrative ductile deformation.

1.4.2 The La Grande subprovince

The volcano-plutonic La Grande subprovince spans the regions bordering the north, west, and south of the Opinaca. It comprises four major lithologic assemblages (Figure 1b), including 3.45-2.8 Ga orthogneiss of the Langelier complex which is locally preserved across the region (Goutier et al., 2000). The ca. 2820 Ma

Guyer Group and the ca. 2730 Ma Yasinski Group (Goutier et al., 2000; Goutier et al., 2001, 2002; Bandyayera et al., 2011, 2014) are volcano-sedimentary successions that largely comprise mafic to bimodal volcanic rocks (Bandyayera et al., 2014). A widespread magmatic even ca. 2719-2709 Ma emplaced the Duncan intrusions (Goutier et al., 1998, 1999a, 2002), and other similar plutons and batholiths throughout the subprovince. Terrestrial to nearshore coarse clastic sedimentary rock sequences overlie the Yasinski and Guyer Groups and are locally sourced (Duparc et al., 2016), lithologically resembling Timiskaming-style sediments. Deposition has been constrained to younger than ca. 2710 Ma (Davis et al., 2014). The volcano-sedimentary sequences form linear belts that exhibit tight synclinal folds between Duncan intrusions, or similarly aged, plutons (dome-and-keel structures). Plutonic bodies are commonly elliptical to irregularly shaped, round or oblate, and can have complex internal foliation patterns. The timing of shear structures, faults, and dome-and-keel structures in volcano-plutonic complexes remain poorly temporally constrained. Crustal slivers of the Langelier Complex exhibit complex deformation from early deformation events (Goutier et al., 2000).

The La Grande subprovince exhibits a metamorphic gradient within its supracrustal rocks, varying from greenschist and lower amphibolite in the west, to granulite in the east (Goutier et al., 1999a, 1999b; Cadéron, 2003; Gauthier et al., 2007; Côté-Roberge et al., 2016). However, the periods of regional metamorphism are poorly constrained. It is suspected that the Langelier Complex underwent a Mesoarchean phase of metamorphism (Goutier et al., 1999b).

Mineral showings outcrop in the La Grande subprovince, notably within the region along its boundary with the Opinaca subprovince (Card and Poulsen, 1998; Gauthier et al., 2007; Ravenelle et al., 2010; Aucoin et al., 2012; Mercier-Langevin et al., 2012; Fontaine et al., 2015). These include orogenic vein hosted gold (lode gold), base metal occurrences, and ultramafic rock hosted Ni-Cu-PGE occurrences (Houlé et al., 2015; SIGÉOM, 2018).

Metasedimentary domains with characteristics similar to the Opinaca metasedimentary subprovince exist within bounds of what is commonly held to be the La Grande. These include the study region in the Lac Joubert region. This region is contiguous to the Opinaca (Fig. 1) and comprises dominantly migmatized paragneiss and orthogneiss, however it also includes stratiform amphibolite, exhalative iron formations, and conglomerates (SIGÉOM, 2018). The orthogneiss, ca. 2704 ± 2 Ma Joubert Suite (Lamothe et al., 2000), exists either as basement to the paragneiss, or as early sills intruded into the sediments (Cadéron, 2003). This region has been labeled a transitional metasedimentary domain in Figure 1, due to the lithologic assemblage bearing similarity to both the La Grande and Opinaca. The major tectonic boundaries that separate this region from the Opinaca complicates the definition of the subprovince boundary, due to the region's similarity to both subprovince types.

1.5 Models of Superior Province formation

The La Grande surrounding the Opinaca on three sides does not fit into some models of Superior Province (Figure 1A) formation and assembly. Early synthesis of lithostratigraphic, geochronological, and geophysical studies have interpreted that the western Superior represents a collage of sequentially accreted terranes (Card, 1990; Calvert et al., 1995). In this model, the alternating, east-west oriented, southward-younging volcano-plutonic and metasedimentary belts represent arc and syn-orogenic flysch basins, respectively (Polat et al., 1998; Percival et al., 2012, and references therein). In the northeastern Superior, the Opinaca does not form a belt, though it does exhibit evidence of convergent deformation. The recent models of Bédard et al. (2003), Bédard and Harris (2014), and Harris and Bédard (2014) explain the

development of the Superior through large-scale events involving the disaggregation of pre-existing continental crust through rifting, with subsequent transition to a phase of reassembly through collision and imbrication of large crustal blocks and slivers. In this model, motion is driven by traction of the mantle against deep cratonic keels.

Both models are constrained by phases of volcanism, metamorphism and deformation: ca. 2780-2720 Ma mafic and ultramafic volcanism occur contemporaneous with localized crustal recycling at concentrations of TTG suite intrusions (Percival et al., 2012); ca. 2720-2680 Ma is a phase of widespread TTG plutonism (Bédard et al., 2003; Simard et al., 2003), with localized collision and convergent deformation zones (Benn et al., 1994), and the development of metasedimentary subprovince basins; ca. 2680-2620 Ma regional metamorphism and transpressional deformation occurred, with metasedimentary subprovinces experiencing low-pressure, high-temperature metamorphism (Corfu et al., 1995; Côté-Roberge, 2018; Piette-Lauzière et al., 2019) and convergent deformation. Deformation has been characterized as broadly dextral transpressional, however partitioned north-south oriented convergent deformation structures are common (Kerrich and Feng, 1992; Polat et al., 1998). Late-phase, orogen-parallel, E-W oriented extension occurred in the southern Superior (Moser et al., 1996). Epigenetic mineralization accompanies late-phase deformation and the transition towards more localized deformation in discrete shear zones under cooler crustal conditions (Kerrich and Feng, 1992; Gauthier et al., 2007; Aucoin et al., 2012; Mercier-Langevin et al., 2012; Bogatu, 2017).

2. Field observations of the Lac Sakami region

Geological mapping in the summer of 2016 was carried out along the La Grande-Opinaca boundary in the Lac Sakami region to examine large-scale structures in greenstone belts. Within this region the geological map pattern of the La Grande appears as a ‘dent’ into the northwest Opinaca, along their generally straight east-west oriented boundary. A total of 114 outcrops were mapped to establish the lithology and structural pattern over the region, with a strong emphasis on the examination of folds and shear zones (Figure 2A). Structural data and outcrop information is publicly available through the Québec government website SIGÉOM (2018). Lithologies in the region include successions of coarse- and fine-grained amphibolite interbedded and interlayered with felsic to intermediate meta-volcanic rocks, volcaniclastic rocks, and metasedimentary rocks (Figure 3A). Porphyroblastic garnet and amphibole are sporadically present in various lithologies (Figure 3B). Included within the successions are gabbroic rocks, however their nature as intrusions, dykes or sills is unknown. Units of diorite exist in the west of the map area, however their relationship with the volcanic successions was not determined. Large Duncan intrusions occupy the northwest portion of the map area. Dykes that compositionally and texturally appear similar to the Duncan intrusions are found throughout the map region. There is one large intrusion of tonalite entrained in the fold pattern is located in the centre of the map.

2.1 Structural domains

The mapped region has been divided into five structural domains based on differences in observed structural and lithological characteristics between shear zone bounded regions (Figure 2B). The map pattern in Domain I is characterized by concentric, elliptical fold enclosures of mafic to felsic meta-volcanic successions and gabbro (referred to below as the “eye fold”). A weakly deformed felsic dyke or volcanic horizon was sampled within the eye fold to constrain the age of the unit and its folding. The axial trace of

the eye fold is oriented east-west and the elliptical enclosure has an approximate 4 to 1 aspect ratio for its E-W length to N-S width. The concentric, elliptical pattern, with both western and eastern fold closures, are visible in aeromagnetic images (Figure 2C; Mouge and Astic, 2013), and the eye fold defines the 'dent' in the La Grande-Opinaca boundary; its axial trace is parallel and aligned with the boundary. A folded tonalite intrusion in part follows the folded volcano-sedimentary successions, however within the western fold closure of the eye fold the intrusion appears thickened, and it traverses the northern domain-bounding shear zone.

Domain II is bounded along its south by a shear zone where in contact with Domain I. It exhibits a network of shear zones that generally trend east-west, with tight folds in some units between shear zones. Sections of the central tonalite body described for domain I exhibits a mushroom fold, likely shear related (Carreras et al., 2005), within bounding metasedimentary units, along the southern domain-bounding shear zone. Within domain II small intrusions of ultramafic rocks are most commonly found as boudins within shear zones. One large outcrop of lamprophyre is present, cross-cutting the regional foliation. Throughout this domain distributed mylonite zones are present, the most concentrated of which are marked as shear zones in Figure 2. However, many thin zones of mylonitic rocks, commonly localized in certain horizons of interbedded units (Figure 3C), provide a measure of the high degree of ductile deformation within this zone. Quartz-feldspar porphyritic dykes with a weakly deformed matrix were observed to cross-cut mylonitic rocks (Figure 3D). Both mylonitic tonalite rocks and the less deformed porphyritic dykes were sampled for geochronology to establish timing of deformation and to constrain the crosscutting relationship, respectively. Gold occurrences are hosted in this domain, within shear zones cutting gabbroic units and parts of the volcanic successions and late vein systems (Figure 3E). One weakly folded dyke was sampled from the margins of the mineralized shear zone to provide a generalized age of late shearing within this domain (Figure 3F).

Domain III exhibits an open to close fold of its entire stratigraphic section, and the fold appears to be rootless. It is in shear zone contact with domains one and two, and its volcano-sedimentary successions terminate against the shear zones. This unit-scale fold is visible in the aeromagnetic map image as repetitive tight gradients between magnetic highs and lows. The units are thicker in the hinge and appear to smear along the shear zone boundaries of the domain. Domain IV represents the Opinaca, South of the boundary with the La Grande, and is not extensive within the map area. Very little analysis was completed for this region, as much of the terrain is covered by marsh. This region exhibits very little internal structure or texture within the aeromagnetic image (Figure 2C). Its northern boundary with the La Grande is defined by a very sharp, continuous magnetic low. Domain V is plutonic rocks of the Duncan intrusions, and apart from its pervasive internal foliation it exhibits little structure.

2.2 Fold structures in outcrop

Folds are common outcrop occurrences within the entire region, both as shear-related intrafolial folds and folds due to bulk flattening. Folds are commonly chaotic in regions with extensive interbedding of layers with strong competency contrasts (Figure 4A), and folds commonly show thickening in the hinges and thinning of limbs. Compositional layering that is presumed to be associated with primary volcanic and volcaniclastic inter-layering is common, exceptionally so in Domains II and III (Figure 3A). Transposition of primary layering into secondary foliations occur in limited regions in proximity to shear zones and along the axial surface traces of major fold structures (Figure 4B). Fine-grained amphibolitic rocks rarely show any indications of folds, however, dykes that intruded these more competent units commonly exhibit tight to isoclinal folds, many of which appear to have folded through passive slip folding (Figure 4C). Folds are

also seen on rare vertical outcrop surfaces, and many finely compositionally interlayered units exhibit very tight to isoclinal folds (Figure 4D).

2.3 Shear zone structures in outcrop

Shear zones within the region exhibit strongly transposed rocks, mylonitic foliations, and associated intrafolial folds. Mylonitic rocks are found along the southern boundary of Domain I where in contact with the Opinaca, and these exhibit a strong down-dip lineation. The network of shear zones within Domain II hosts mylonites within more competent tonalite and gabbro units. These mylonites exhibit C-S and C' fabrics, and σ-type asymmetric porphyroclast structures on surfaces parallel to the elongation direction and perpendicular to the foliation (Figure 4E). They also exhibit strong ductile stretching and mineral elongation lineations, that are generally down-dip (Figure 4F). Rare occurrences of outcrop scale elliptical fold closures, tentatively interpreted as sheath folds, were observed in proximity to shear zones. Figure 5A shows one such outcrop of finely thinned mafic and felsic compositional interlayering that exhibits numerous isoclinal folds and elliptical fold closures (schematic diagram in Figure 5B). Isoclinal fold closures are also visible on a cross-sectional vertical surface of the same outcrop (Figure 5C). Its proximity to the La Grande Opinaca boundary within Domain I, which exhibits map-scale elliptical fold closures, demonstrates the independence of scale for these structures. These isoclinal and sheath folds may indicate large-scale shearing was responsible for localized fold development in regions close to shear zones.

3. Structural analysis of the Lac Sakami region

3.1 Stereonet analysis

Measurements of compositional layering and schistosity orientations taken from outcrop were compiled for analysis. Mylonitic foliations and dyke orientations were also measured, as well as linear structural features including outcrop scale fold hinges, and mineral elongation lineations associated with L-tectonites or mylonitic rocks. Representative measurements are indicated on Figure 2, and summaries of all measurements by domain are plotted on stereonets in Figure 6.

Compositional layering within Domain I show a strong concentration or cluster towards steeply north dipping (Figure 6A). The spread of their orientations varies towards steeply east and west dipping. Measurements from both north and south of the east-west oriented axial surface trace of the eye fold of Domain I (Figure 2) dip in the same direction, towards the north. Measurements for each limb are very similar, and the overall orientation of each limb is nearly indistinguishable from the other. Both limbs are nearly parallel with measured axial planar cleavages and axial planes of outcrop scale folds. This is indicative of an overturned isoclinal fold. The calculated fold axis from the cylindrical best fit plunges approximately 60° towards the North. Mineral elongation lineations measured in this region form a cluster around this calculated fold axis. However measured fold axes are evenly distributed throughout the general orientations of measured axial planes. Measured axial planes show a spread of orientations from steeply to moderately north dipping. Mylonitic foliations and dyke orientations are generally parallel to axial planes.

Compositional layering within Domain II forms a broad cluster generally parallel with the axial planes of Domain I (Figure 6B). Mylonitic foliations are generally parallel to this as well. Their associated mineral stretching elongation lineations plunge steeply to moderately towards the North, generally down-

dip on the respective mylonitic foliation. Dyke orientations vary from being parallel to local layers, to striking north-south with steep dips.

Compositional layering from Domain III exhibit a broad distribution of steeply dipping orientations, striking South East to North and a generally dipping towards West to North (Figure 6C). The fairly even distribution is spread along the best fit profile plane, a pattern consistent with the open to close, round folds observed in the map pattern (Figure 2). North and south limbs of the fold dip in the same direction, and similar to Domain I, this fold is likely overturned. Mylonitic foliations are not numerous, but are generally parallel with layering. The calculated fold axis plunges steeply towards the Northwest. Mineral elongation lineations cluster around this calculated fold axis. Scant measured outcrop fold axes cluster plunge steeply towards the Northeast.

Within domain IV the regional foliation dips moderately to steeply towards the North (Figure 6D). A small number of mineral elongation lineations were measured along the Opinaca-La Grande boundary, and these are generally oriented down-dip along the foliation, plunging moderately towards the North. Domain V exhibits similarly oriented foliations (Figure 6E), however, this region was not mapped extensively.

In summary, foliation orientations dominantly cluster around an East-West to East-northeast-West-southwest strike, with a moderate to steep dip towards the Northwest to North. Mylonitic foliations are generally parallel to both the cluster of foliations and axial planes for the region (Figure 6F). Mineral stretching elongation lineations throughout the entire region forma cluster that plunges moderately to steeply towards the North-northwest. There is minor variation between the domains, but lineations generally follow the pattern of being down-dip on their respective foliation. Fold axes throughout the region are generally spread throughout the range of axial plane orientations.

3.2 Kinematic analysis

Petrographic studies of mylonitic rocks show that porphyritic volcanic, and phenocrystic plutonic rocks, provide microstructural kinematic indicators. The temperatures and magnitude of ductile shear strain formed porphyroclastic σ-type structures from phenocrysts in metavolcanic (Figure 7A) and metaplutonic rocks (Figure 7B). Figure 7A exhibits relict porphyroclasts of sericitized phenocrysts, presumably pseudomorphing previous plagioclase. Asymmetric tails of recrystallized quartz, in the context of their oriented sample, are consistent with a north-over-south (thrust) sense of motion for the shear zone bounding domains two and three. Static recrystallization textures of quartz mantling the porphyroclast indicate a degree of metamorphic strain recovery. Figure 7B exhibits a σ-type porphyroclastic plagioclase grain, partially dynamically recrystallized around its grain boundary, with asymmetric tails of fine quartz grains. We interpret these tails to have formed in strain shadows, and to indicate a north-over-south thrust sense of motion for northern shear zones in domain II. Figure 7C exhibits numerous σ-type porphyroblasts or porphyroclasts of amphibole in a fine quartz and plagioclase matrix. The amphibole grains have irregular grain boundaries along the terminations at their apparent long axis. At these sites collections of matrix have formed asymmetric tails. We interpret these tails to have formed in strain shadows, and to indicate a south-over-north sense of motion. However, some of these kinematic indicators are nearly symmetric, and this sample exhibits some opposing kinematic indicators. Its overall sense of motion may be ambiguous, but as interpreted it is an opposing, normal sense of kinematics for the boundary between domains one and two.

4. Field observations of the Lac Joubert region

Geologic mapping in the summer of 2015 was carried out by a team of MERN geoscientists to map three SNRC map sheets. The analysis below provides additional structural context beyond the geologic mapping efforts, reports for which will be forthcoming by MERN. Figure 8A shows a simplified geologic map of the entire region. Within this region the La Grande borders the Opinaca, and their contact is located in the southwest of the map region. The La Grande rocks in this region differed greatly from the typical volcano plutonic complexes. Migmatized paragneiss surrounds folded units of orthogneiss and foliated tonalite. One large late felsic pluton occupies the Eastern portion of the map. Paleoproterozoic dykes, generally oriented north-south, traverse the region.

4.1 Structural domains

The region has been divided into three structural domains, each with a distinct structural style. They are separated by two parallel ductile shear zones, the Orillat shear zone between the Opinaca and Boisbriand (domains I and II), and the Pradier shear zone between the Boisbriand and the La Grande (domains II and III). Domain I comprises entirely paragneiss, migmatites, and leucocratic injections, lithologies that are common within the Opinaca. Domain II comprises strongly deformed paragneiss and northwest-southeast striking irregular units of orthogneiss and foliated tonalite. Domain III comprises orthogneiss that exhibits elliptical fold closures, and an overall map scale pattern of unit faults. Paragneiss occupies the remainder.

4.2 Fold structures

Folds within Domain I, the Opinaca, vary from open to close at the outcrop scale, where folding is observed within compositional layering (Figure 9A). Leucocratic injections commonly exhibit chaotic ptygmatic folds (Figure 9B). Folds within Domain II are most commonly observed within layered leucosome, however they can be observed folding the regional foliation in paragneiss. Folds commonly exhibit asymmetric strongly thinned limbs, and thickened hinges. On vertical surfaces they are observed as close to isoclinal folds, commonly overturned when tight to isoclinal (Figure 9C). Some hinges show progressive refolding through normal sense stretching and shearing (Figure 9D). Within Domain III orthogneiss can exhibit complex fold patterns (Figure 9E) and leucocratic injections in paragneiss exhibit upright open to close folds (Figure 9F).

4.3 Shear zones

Regional shear zones in high-grade paragneiss units are difficult to identify on outcrop. They can be characterized as sites of extensive migmatization exhibiting tightly spaced, very straight and parallel layers of leucocratic injections and migrated leucosome (Figure 10A). Both the Orillat and Pradier shear zones (Figure 8A) are very wide, at a scale of hundreds of meters, although due to the high-grade nature their exact width is difficult to establish as deformation fades slowly into very similar looking migmatitic rocks. At the approximate centre of the Pradier shear zone (Figure 10A and 10B) isoclinal overturned folds in stromatic migmatite layers are common and exhibit a southward vergence of their axial surface. Some folds may indicate a component of dextral sense of strike-slip shearing along the shallowly north dipping shear zone (Figure 10B). The Orillat shear zone can be similarly characterized, with exceptionally straight,

parallel migmatite layering. Very rare σ-type shear structures were observed (Figure 10 C and D) that exhibit a dextral sense of strike-slip shear along the shallowly north dipping shear zone. These structures are formed from leucosome in paragneiss.

Domain III exhibits a pervasive, penetrative east-west oriented ductile regional foliation. Distributed throughout the units of orthogneiss are local shears oriented northwest-southeast that deflect the regional foliation in a dextral sense (Figure 11A). They are commonly found in the meter scale, and many such structures can be found in single outcrops. They are common throughout the region. With the context of dextral deformation observed in shear zones, this orientation is consistent with a C' orientation from east-west oriented dextral shear. Late dextral shears were observed in the La Grande oriented northwest-southeast (Figure 11B), however the shear zones are rare, isolated, only meters thick, and do not appear to have defined the map pattern in any way.

5. Structural analysis of the Lac Joubert region

5.1 Stereonet analysis

Structural data compiled from the summer's work for the entire team is plotted, by domain and by structure type (folds and shear zones), on stereonets in Figures 12-14. Domains I and II exhibit similar styles of folds. Domain I, the Opinaca, exhibits a spread of poles to gneissosity and stromatic migmatite layers with two concentrations (Figure 12A). The poles to foliations are organized along a north-south trending steeply West dipping profile plane, with a calculated axis plunging shallowly towards the east. Measured axial surfaces dip towards the North and are coincident with the calculated fold axis, and are consistent with the two clusters of poles to foliations being limbs of the fold (Figure 12B). Scant measured fold hinges cluster around the calculated fold axis. The interlimb angle is approximately 75° (Figure 12B). Domain II exhibits similar orientations of poles to gneissosity and stromatic migmatite layers, however the poles are concentrated in an orientation steeply to moderately north dipping (Figure 12C). This is consistent with field observations of overturned tight to isoclinal folds, where both limbs occupy nearly the same region on the stereonet. The profile plane is similarly oriented to Domain I, with a similar calculated fold axis. Numerous fold axis measurements cluster around the calculated axis, however there is some spread (Figure 12D). Measured axial surfaces are generally oriented east-west and very from steeply to shallowly dipping. The interlimb angle is estimated to be 30° from two maxima in the tight cluster of measurements. Both Domain I and Domain II are consistent with folds caused by regional N-S shortening, with shallowly eastward plunging fold axis (Figure 12E). Folds within Domain II are tighter, and overturned, but otherwise similarly oriented.

Measurements of orthogneiss, paragneiss, and stromatic migmatite layers from Domain III exhibit a much wider set of orientations (Figure 13A). The stereonet of their poles to foliations shows concentrations of steeply dipping east-west oriented planes, similar to domains I and II, however the numerous measurements show a very wide spread from these centres. A cylindrical best fit profile plane is similarly oriented to domains I and II, steeply dipping towards the West. The calculated fold axis plunges shallowly towards the East. In stark difference to Domains I and II, measured fold axes show a large spread from East to West through a set of vertical east-west oriented great circle (Figure 13B). The spread of these axes is compatible with folding about a north-south axis. This second generation of folds may be conical, providing the wider spread of the fold axis measurements along the profile plane the second-generation fold (Figure 13C). The wide spread of foliations is also consistent with an interpretation that a second-generation

of folding spread foliation planes poles in an east-west fashion about a north-south axis. This analysis is consistent with the first generation of folds that were upright, open to close, slightly eastward plunging, over-printed by a second generation of open and upright folds with a subhorizontal north-south axis (Figure 13D).

Structural data of mylonite foliations, and flattening foliations (all MERN foliation data with deformation category ≥4; SIGÉOM, 2018), and the associated mineral elongation lineations for shear zones are plotted in stereonets in Figure 14. The Orillat shear zone has mylonite foliations dipping shallowly to moderately towards the North to Northeast. The associated mineral elongation lineations plunge shallowly to the east to southeast. Migmatite layers measured within the shear zone exhibit a cluster that dips moderately northwards, but with a spread that is consistent with folds patterns seen within domain II. The Pradier shear zone exhibits mylonite foliations dipping moderately to steeply towards the North-northeast. Few measurements dip towards the Southwest. Mineral elongation lineations associated with the foliations generally plunge shallowly towards the east to southeast, however, some plunge moderately to the Southeast and few plunge steeply to the south.

6. Geochronology

Four igneous samples were analyzed for U-Pb zircon geochronology from the Lac Sakami region study area. Within the Lac Joubert region, two samples of paragneiss and one granodiorite were taken from the Opinaca, and four paragneiss samples were taken from the La Grande, all for U-Pb zircon and monazite geochronology.

In the case of the Lac Sakami region, dykes representing various phases of the structural history (pre-, syn-, and post deformation) were sampled to place constraints on deformation for their respective units. Such relationships are rarely observed in outcrop, and samples were commonly taken from small or thin units; hence, as thin dykes, a degree of contamination or inheritance is expected.

Considering that dating regional folding is difficult absent of large-scale cross-cutting relationships, our strategy for establishing the timing of deformation within the Lac Joubert region is to use monazite and metamorphic zircon (Th/U ratio < 0.1) U-Pb ages separated from migmatized and high-grade paragneiss to establish periods of near-peak metamorphism. This provides a proxy age for the crustal thickening that likely accompanied first generation folds developed from N-S shortening. These are accompanied by two additional igneous age constraints to place further constraints on specific phases of deformation.

Samples were processed for laser ablation inductively coupled plasma mass spectrometry (LA-ICPMS) U-Pb detrital zircon geochronology by D.W. Davis at the Jack Satterly Geochronology Institute at the University of Toronto in Ontario, Canada.

6.1 Analytical methodology

Electroshock disaggregation and subsequent panning at the Overburden Drilling Incorporated laboratories concentrated samples 15-HH-2100, 15-FB-7519, 15-SB-3098, 15-CL-5111, 15-NC-6124, 15-NC-6050, and 15-NC-6127. Samples 16-NC-4676-B, 16-NC-4676-D, 16-NC-4700E, and 16-NC-4645-D were crushed using a jaw crusher and further pulverized by a disk mill. Additional separation of heavy minerals for these samples was carried out with a Wilfley table. All samples were subjected to paramagnetic

separation with the Frantz isodynamic separator and density separations using bromoform and methylene iodide. Final sample selection for geochronology was by hand picking under a microscope, choosing the freshest, least cracked zircon and monazite grains. Both types of grains were imaged with backscattered electrons (BSE) using a JEOL JSM6610-Lv scanning electron microscope. BSE images of representative grains, with their target spot analysis locations, are provided in Figures 15 (Lac Sakami region samples) and 16 (Lac Joubert region samples). Cathodoluminescence (CL) imaging was not used because most sampled zircon grains are altered and damaged by radiation, which suppresses their luminescence, and monazite does not fluoresce.

Imaged monazite and zircon grains were partially ablated using a 213 nm New Wave laser at 5 Hz and about 5 J/cm^2 with beam diameter of 25 microns for zircon. Mass spectrometry was carried out on a Plasmaquad quadrupole ICPMS. Data were collected on 88Sr (10 ms), ^{206}Pb (30 ms), ^{207}Pb (70 ms), ^{232}Th (10 ms) and ^{238}U (20 ms). Prior to analyses, spots were pre-ablated with a larger beam diameter for 1 second to clean the surface. Following a 10 sec period of baseline accumulation, the laser sampling beam was turned on and data were collected for 25 seconds followed by a 40 second washout period. About 140 measurement cycles per sample were produced and ablation pits are about 15 microns deep.

Data were edited and reduced with custom VBA software written by D. W. Davis. ^{206}Pb/^{238}U ratios show increasing fractionation caused by penetration depth through the run while the ^{207}Pb/^{206}Pb profile is usually flat. No corrections were made for common Pb, since the ^{204}Pb peak is too small to be measured precisely, and common Pb should be insignificant for unaltered Precambrian zircon and monazite. Levels of ^{88}Sr were monitored from zircon analyses in order to detect intersection of the beam with zones of alteration or inclusions; data showing high Sr or irregular time resolved profiles were either averaged over restricted time windows or rejected.

Two zircon standards were measured, bracketing sets of four sample measurements. The standards DD85-17, from a quartz diorite from the Marmion batholith in northwest Ontario previously dated at 3002 +/- 2 Ma by isotope dilution thermal ionization mass spectrometry (ID-TIMS; Tomlinson et al., 2003) and DD91-1, a monzodiorite from the Pontiac province of Québec dated at 2682 ± 1 Ma (Davis, 2002) were used. The monazite standard was from DD90-26A, a sample of the Lac LaCroix granite in the western Superior Province of Minnesota previously dated at 2671 +/- 2 Ma (D.W. Davis unpublished data). Differences between standards are time interpolated to correct sample measurements.

6.2 Sample descriptions and analytical results summary

Results of U-Pb isotopic analyses by LA-ICPMS for Lac Sakami region samples are provided in Table 1. Results of for Lac Joubert region samples are provided in Table 2. Concordia diagrams for all zircon spot analyses of each sample from the Lac Sakami region are provided in Figure 17. Concordia diagrams for all zircon spot analyses of each sample from the Lac Joubert region are provided in Figures 18-20. Concordia diagrams were calculated by and plotted using the program Isoplot of Ludwig (1998, 2003). U decay constants are adopted from Jaffey et al. (1971).

6.2.1 Lac Sakami region sample descriptions and results

16-NC-4676-B Foliated tonalite dyke

A strongly foliated tonalite dyke parallel to layering in Domain II was sampled establish the youngest possible age of deformed rock in the region (this unit is crosscut by 16-NC-4676-D, below; Figures 3C and 3D). BSE of zircon images show a uniform zircon population characterized by oscillatory zoning (Figure 15A). U-Pb analyses on zircon indicate a uniform age with an average of 2838 ± 5 Ma (MSWD – 1.4). This is the best estimate for crystallization of the dyke.

16-NC-4676-D Porphyritic felsic crosscutting dyke

Sampled from the same outcrop as 16-NC-4676-B, this quartz-feldspar porphyritic dyke crosscuts the local foliation (Figures 3C and 3D), including the foliation associated with 16-NC4676-B and adjacent mylonitic gabbro. This sample yielded only a small amount of zircon. Grains are euhedral prisms, generally cracked but fairly fresh and appear to represent one population. BSE images show that most grains have oscillatory zoning in many cases with possible cores and overgrowths that are both zoned (Figure 15B). The results of U-Pb analyses show that most data cluster within error, giving an average age of 2835 ± 5 Ma (MSWD – 0.8), the same as that of the 16-NC-4676-B tonalite dyke (Figure 17B). However, some data are distinctly younger with the three youngest overlapping with an average $^{207}Pb/^{206}Pb$ age of 2727 ± 11 Ma. All analyses have Th/U ratios within the range expected for magmatic zircon (Table 1) but most grains are clearly xenocrystic. The youngest age may date crystallization of the dyke but may also be an older age estimate if these grains are also xenocrystic.

16-NC-4700-E Felsic dyke or volcanic layer

This sample is a felsic dyke or volcanic layer located within the stratigraphic succession of the eye fold in Domain I. It was sampled to constrain the age of the units, and possibly deformation; it is weakly deformed with respect to the surrounding rocks, however, this may be due to a competency contrast.

Zircon in this sample form a uniform population of stubby sharply terminated euhedral fresh grains. BSE images show a consistent pattern of fine oscillatory zoning in most grains (Figure 15C). Uniform unzoned regions with euhedral boundaries in the middle of grains are probably areas where the plane of polishing is subparallel to a crystal plane.

U-Pb analyses are near-concordant (Figure 17C) and clustered but scatter slightly outside of error with an average $^{207}Pb/^{206}Pb$ age of 2740 ± 5 Ma (MSWD – 1.6). There is no obvious indication of a two differently aged populations. The oldest 7 analyses are on uniform cores that lack the characteristic oscillatory zoning of the main population. Omitting these leaves an average of 2737 ± 4 Ma (MSWD – 1.0) and the data scatter within error. This may be a slightly better estimate for the age of dyke emplacement.

16-NC-4645-D Folded tonalite dyke crosscutting gabbro mylonite

This sample was taken from the margins of a discrete shear zone in gabbro of Domain II, along the boundary with Domain I. The tonalite dyke sampled is closely folded, and generally less deformed than the rocks hosting it (Figures 3E and 3F). It was analyzed to provide a date of late stage, or waning shear zone deformation.

The sample yielded a small amount of generally cracked and altered zircon. BSE images show a variety of zoning patterns and the possible presence of cores in some grains (Figure 15D) but cores do not

seem to be preferentially older (Table 1). U-Pb data are near-concordant and scatter somewhat outside of error (Figure 17D) with an average $^{207}Pb/^{206}Pb$ age of 2727 ± 7 Ma (MSWD – 2.6). Arbitrarily dividing the data into younger and older age groups (shown as different coloured ellipses on Figure 17D) gives average ages of 2711 ± 7 Ma (MSWD – 0.6) and 2737 ± 7 Ma (MSWD – 0.8). This may indicate that a cognate population of zircon is mixed with xenocrysts similar in age to 16-NC-4700-E, and the younger age provides the best estimate for emplacement.

6.2.2 Lac Joubert region sample descriptions and results

15-HH-2100 Paragneiss

Monazite grains from 15HH2100 are featureless under BSE so images are not included. Two U-Pb data scatter somewhat outside of error but six others overlap and all the data define an average $^{207}Pb/^{206}Pb$ age of 2652 ± 12 Ma (Figure 18A). This is likely an age of metamorphism.

15-FB-7519 Paragneiss

This sample yielded only a few small grains of monazite. Polished monazite grains are small and featureless under BSE (Figure 16A). Analyses of 7 out of 10 grains produced near-concordant overlapping data with an average $^{207}Pb/^{206}Pb$ age of 2647 ± 6 Ma (Figure 18B), which is the best estimate for the age of high-grade metamorphism. Three other grains gave older ages with the oldest being 2756 ± 18 Ma and strongly reversely discordant. These may be detrital grains but may also have been affected by common Pb, since some grains were not clear and fresh-looking.

15-SB-3098 Granodiorite L-tectonite

This sample yielded only a small amount of highly damaged zircon grains, generally as long prisms (Figure 16B) but it also has a robust population of monazite. Its long prismatic zircon grains have longitudinal cracks, a common result of radiation induced expansion, which may have promoted alteration as fluid pathways. Consequently, only few spots were targeted, and of eighteen acceptable analyses all show age scatter with variable discordance (Figure 18C). The youngest near-concordant spot gives an age of 2711 ± 18 Ma (Table 2). A cluster of monazite data gives an average age of 2678 ± 8 Ma. Metamorphic monazite is not expected in a rock of this composition so this may represent the crystallization age of the granodiorite; magmatic crystallization should at least be bracketed between the age of the monazite and that of the youngest zircon.

15-CL-5111 Paragneiss

This sample yielded both zircon and monazite. Zircon grains are generally cracked with turbid altered overgrowths. BSE images (Figure 16C) confirm the presence of high-U overgrowths on many of the zircon grains. These rims generally provide young ages and show relatively high-U and low Th/U (<0.1), characteristic of metamorphic zircon. The four youngest spots establish an age of 2640 ± 6 Ma for growth of the rims (Figure 19B). The sample contains fresh monazite crystals, which show a range of colours from pale green, which is common for monazite, to dark. BSE images from both groups (Figure 16D) show relatively dark cores. Both data sets are near-concordant but $^{207}Pb/^{206}Pb$ ages scatter slightly outside of error

and there is no obvious relationship between the ages of cores and rims. Three analyses from the greenish clear monazite population give overlapping older ages with an average of 2705 ± 12 Ma (Figure 19A) but these appear to be on rims. The other analyses overlap with an average of 2652 ± 5 Ma. The group of darker monazite analyses show some scatter but omitting 3 analyses leaves an overlapping group with an average age of 2634 ± 4 Ma, which is distinctly younger than the first group. One interpretation might be that growth of monazite occurred over a protracted time period, in phases beginning at 2705 Ma (unless the older monazite grains are detrital), and ending at about 2634 Ma, close to the time of metamorphic zircon growth.

15-NC-6124-A3 Parageiss with leucosome

This sample yielded a small amount of tiny monazite grains. BSE images of monazite are featureless (Figure 16E) but U-Pb analyses show a range of concordant ages well outside of error from 2596 ± 12 Ma to 2707 ± 14 Ma (Figure 19C). The U concentration of the spots shows a clear inverse correlation with age (Figure 19C bottom), which suggests that monazite formed over a period of at least 100 Ma from increasingly evolved fluids.

15-NC-6050 Paragneiss with leucosome

BSE images of polished monazite show generally darker or splotchy cores with lighter overgrowths (Figure 16F). All U-Pb analyses on monazite produced concordant data (Figure 19D) but these scatter outside of error from 2633 ± 18 Ma to 2709 ± 20 Ma (Table 2). The data can be divided into two overlapping clusters with average ages of 2656 ± 4 Ma and 2697 ± 9 Ma, based on just 4 data (Figure 19D). There is a rough inverse correlation between U concentration and age, which might be expected in a progressively crystallizing system where the most evolved liquid should have the highest U concentration.

15-NC-6127 Deformed pegmatite dyke

Sample 15-NC-6127 is from a deformed pegmatite dyke that exhibits dextral shearing and mylonitic textures. It was sampled to provide an age constraint on localized, discrete shearing in dextral shear zones within Domain III.

This sample yielded cracked dark-brown zircon, which is usually an indication of high U concentration, as well as large grains of monazite. BSE images show that many zircon grains contain cores overgrown by a high-U (bright) phase (Figure 16G). U-Pb analyses with magmatic Th/U signatures give a range of ages from 2694 ± 16 Ma to at least 2927 ± 18 Ma (Figure 20A). The youngest analyses all show low Th/U metamorphic or hydrothermal signatures, which is typical of zircon crystallized in pegmatite and aplite. The youngest is 2592 ± 14 Ma but the time-resolved analysis profile shows slightly high Sr and a tendency for the age to increase with decreasing Sr. The $^{207}Pb/^{206}Pb$ ages of four other low Th/U analyses overlap with an average of 2636 ± 7 Ma. This is the best estimate for the age of zircon crystallization in the pegmatite. Monazite grains are relatively large and show slight amorphous variations in brightness under BSE (Figure 16H). U-Pb analyses overlap on or near concordia with an average age of 2625 ± 5 Ma (Figure 20B). This is slightly younger than the zircon and may indicate that monazite saturation was relatively late compared to zircon.

7. Discussion

7.1 Interpretation of structures within the Lac Sakami region

Domain one exhibits a map-scale elliptical fold trace with characteristics that are compatible with it being a large-scale doubly plunging shear-related fold, possibly a sheath fold, as it is bound by shear zones to the north and south of the entire structure. The high aspect ratio of the elliptical trace is consistent with sheath-folds in amphibolite grade metamorphic rocks (Alsop and Holdsworth, 2006; Alsop et al., 2007). The mushroom fold of tonalite along the domain I and II boundary is also consistent with shear-related deformation (Carreras et al., 2005). Domain I exhibits common outcrop-scale isoclinal folds and rare sheath folds, yet there are no focused high strain or shear zones within the eye fold. However, the localized shear zones bounding the domain to the north and south, and the network of shear zones in domain II to the north, may have accommodated high magnitudes of north-over-south oriented dip-slip motion. In this interpretation more homogeneous shear strain, with a component of N-S shortening and upward vertical extrusion, was the mechanism for folding within domain I. This would be consistent with the lack of shear structures within the eye fold, and its relatively lower degree of strain than domains to the north. Initial folds with east-west oriented axial traces would have been modified through progressive deformation, imparted through prolonged slip and southward transport in domain II, to form the doubly-plunging eye fold. The spread of fold axis lineation orientations throughout the axial surface is consistent with the rotation of parasitic fold axes as passive linear markers towards the slip direction due to prolonged shearing. This is an indication of passive slip folding, considering that the axial surface of the fold is parallel to shear zones in domain II, and along the southern boundary of domain I with domain IV. Mineral elongation lineations on mylonitic foliations throughout domain II are consistently down-dip, indicating a high magnitude of shear strain or extrusion (Jiang, 2014). The most consistent microstructural kinematic indicators provide a north-over south sense of motion, therefore we interpret domain II to represent a southward directed thrust system. Observed inconsistent and ambiguous kinematic indicators may be due to back-thrusts, or ductile high-strain zones with a large flattening component. The large-scale fold structure in domain III is a compatible antiform to the style of fold in domain I, as it is overturned and smeared against the boundary with domain II to the east. This array of fold structures are not consistent with fold superpositioning, as domains II, IV, and V exhibit no structures indicative of regional E-W shortening. Within the eye fold there is no evidence of an overprinted N-S foliation, nor fold interference patterns on vertical surfaces that would suggest the structure is a type 2 fold interference pattern.

The U-Pb zircon geochronology presented here provides constraints on the ages of units as well as the timing of deformation within this map region. Within domain II strongly foliated tonalite (sample 16-NC-4676-B; 2838 ± 5 Ma) dyke within mafic volcanic rocks provides an age slightly older than known Guyer group volcanic rocks. This constrains the volcanic rocks to older, but detrital geochronology of the Opinaca (Cleven et al., in prep.) from the region indicate the oldest significant peak of magmatism in the La Grande was ca. 2840 Ma, which was likely associated with rocks of this unit, and continued through Guyer group volcanic ages. Within domain I a weakly deformed felsic dyke or volcanic layer (sample 16-NC-4700-E; 2740 ± 5 Ma) provides an age common with Yasinski group volcanics (ca. 2730 Ma). This age relationship between domains is compatible with the kinematic and structural interpretation that domain II (and III) was thrust over domain I, thus imbricating ca. 2840 Ma volcanic successions (Guyer group), overtop of Yasinski group volcanics. The deeper, possible Guyer group volcanics underwent pervasive ductile deformation during prolonged thrust-sense shearing, and the shallower Yasinski group volcanics were tightly to isoclinally folded, overturned, and progressively sheared to a moderate degree. Deformation timing constraints are provided by the cross-cutting, weakly deformed dyke in domain II (sample 16-NC-

4676-D; 2727 ± 11 Ma), and the folded tonalite dyke sampled from the margins of the shear zone separating domains I and II (sample 16-NC-4645-D; 2727 ± 7 Ma). This age of 2727 Ma could be seen as an earliest constraint for deformation, considering that geochronology analysis of both dykes show large populations of inherited zircon grains. It is unknown if their youngest ages represent inherited zircon as well. A subset of the youngest zircon dates in sample 16-NC-4645-D provide an age of 2711 ± 11 Ma, similar to Duncan intrusion ages, with the remainder providing a Yasinski group compatible age of 2737 ± 7 Ma. Therefore, we interpret that deformation likely occurred contemporaneous with Duncan intrusion emplacement, ca. 2710 Ma, or shortly thereafter. Undeformed lamprophyre dykes sampled nearby in the region have been dated at 2689 ± 7 Ma (Roman Hanes, pers. comm., 2018; ID-TIMS titanite, data unpublished), which constrains definite termination of this deformation.

Deformation described above was likely part of a regional event. The E-W axis of the eye fold, similarly oriented to the shear zone systems surrounding it, may define a regional deformation orientation. Linear E-W structures somewhat evenly spaced throughout the eastern La Grande may therefore have initially developed during an early phase of convergent deformation. An episode of dextral transpression have been described affecting both the La Grande and Opinaca at a regional scale, for which major shear zones exist just north of the Lac Sakami region map area (Cleven et al., 2019). Locally, E-W oriented convergent deformation structures may be either have been created earlier and were preserved due to their favourable orientation, or could have resulted from partitioning of dextral transpressional deformation into a convergent component in the Lac Sakami region, and more focused dextral deformation elsewhere.

7.2 Interpretation of structures within the Lac Joubert region

The Lac Joubert region map is divided into three domains which individually exhibit structures associated with different deformation and tectonic processes, and these domains are separated by the Pradier and Orillat dextral strike-slip shear zones. Regional folds have many important characteristics that differ between domains yet have the consistent feature of a general shallowly eastward plunge (for 1st generation folds in domain III). This indicates that the processes for folding may have differed, yet they formed in the same event. The Boisbriand (domain II) is the most exceptional for 1st generation folds, as folds within the domain are consistently overturned and tight to isoclinal. The intensity and characteristics of its folds, and it being a narrow transition zone sandwiched by shear zones between lithotectonic assemblages of the Opinaca and the La Grande, imply that the Boisbriand is a deformation zone that accommodated focused convergent deformation, possibly due to the La Grande overriding the Opinaca. However, the amount of structural data from the Opinaca (domain I) is limited, and it is possible that it exhibits deformation like the Boisbriand. The Pradier and Orillat shear zones likely accommodated dip slip thrust or oblique motion during high-grade tectonometamorphism, prior to late dextral shearing that defined their lineation patterns and kinematic indicators. High grade metamorphic rocks reset strain readily, and their lineation patterns are a shallowly east plunging cluster consistent with pure strike-slip motion, likely their latest state of strain. Shear zones steepen northward from the shallowly north dipping, southern Orillat shear zone; this is consistent with steepening due to tectonic imbrication during thrust tectonics (Figure 8B).

Second generation folds in domain III have near north-south oriented axial traces, yet these do not cross the Pradier shear zone and domains I and II do not exhibit this generation of folds. This implies that the Pradier shear zone acted as a detachment along which slip could occur to allow bulk E-W shortening of domain III. This shortening is compatible with a homogeneous deformation of the region contemporaneous with dextral strike-slip motion along the Pradier shear zone, thus not affecting the Boisbriand domain.

Metamorphic monazite and zircon reported here provide an interpretation that prograde metamorphism occurred in three separate events. Samples from domains II and III have Concordia ages that are within error of each other indicating a metamorphic event ca. 2700 Ma (Figure 21). The monazite from these analyses are likely detrital, as they predate the age of sedimentation (Cleven et al., in prep.), yet their consistent ages roughly correlate to the timing of convergent deformation in the Lac Sakami region, as outlined above. This supports interpretation of an early convergent event that affected the La Grande, the likely provenance of the paragneiss sample (Cleven et al., in prep.). Four samples, representing all domains, have Concordia ages that are within error of each other indicating a metamorphic event ca. 2652 Ma (Figure 21). This is the most likely period for folding in domains I and II, and 1st generation folds in domain III, all associated with convergence and crustal thickening. This timing is approximately 10-15 m.y. later than the earliest estimates of peak metamorphism by Morfin et al. (2013) in the western Opinaca. One sample in domain III provides monazite and zircon ages that are within error indicating a metamorphic event ca. 2636 Ma (Figure 21). While evidence of this event is found only in domain III, previous studies of the Opinaca have recognized a metamorphic event at a similar time (Morfin et al., 2013). Within domain III, this event could be due to a second crustal thickening event such as the E-W shortening in the overriding plate associated with the 2nd generation of folds. Dextral deformation along the shear zones is constrained as later than a 2678 Ma L-tectonite granodiorite with its lineation parallel to shearing (sample 15-SB-3098), and waning at ca. 2625 Ma from a sheared pegmatite (sample 15-NC-6127). Therefore, a period of dextral shearing and 2nd generation folding is estimated to have occurred between 2635 and 2625 Ma, with deformation waning thereafter. Further west along the Orillat shear zone pegmatites in discrete dextral shear zones have been dated at 2614 Ma (Bogatu, 2017). Tectonometamorphism could even be interpreted to have continued until ca. 2600 Ma, from evidence provided by sample 15-NC-6124, discussed below.

Monazite from sample 15-NC-6124, which is located along the Pradier shear zone, show a near continuous trend of monazite ages from 2707 to 2596 Ma with a correlating linear increase in uranium content (Figure 19C). This could be an indication that metamorphism was long lived and continuous, and in other samples monazite growth was punctual. However, this sample was taken from within a major shear zone, and the effects of fluid and heat transfer through shear zones could be a complicating factor for such an interpretation.

7.3 Tectonic event timeline summary for both Lac Sakami and Lac Joubert regions

The relative sequence of deformation phases in at least one, prolonged, multi-phase tectonic event can be loosely placed on an absolute timescale. Various radiometric dates from literature are referenced to build a timeline of these phases:

- 2727-2711 Ma Deformed dykes in Lac Sakami region, this study – deeper volcanic rocks, possibly Guyer group, with ca. 2838 Ma tonalite, are thrust over Yasinski group volcanics (ca. 2740 Ma) along E-W oriented shear zones, creating large-scale convergence-related fold and shear zone structures.
- 2716-2709 Ma Duncan intrusions (Goutier et al., 1998, 1999a, 2002) and similar plutonic rocks – all dome and keel structures in volcano-plutonic complexes post-date the formation of this suite.
- 2710 Ma, Pluton de la Frégate (Augland et al., 2016) – tonalite pluton located within the metasediments of the Opinaca, constraining the earliest ages of the sedimentary basin.
- 2704 Ma Polaris batholith (Augland et al., 2016) – large, round intrusion (in map view) within the eastern La Grande. This pluton truncates some E-W linear structures in the La Grande, yet also

appears deformed along others. This may indicate that N-S shortening occurred during separate convergent deformation events prior to its intrusion and after.

- 2700 Ma Detrital monazite from paragneiss, this study – a metamorphic event is implied at this time due to monazite Concordia ages from different samples that are within error of each other. This event likely affected the La Grande, the provenance of the paragneiss.
- 2670 Ma Low pressure, high temperature metamorphism (Côté-Roberge, 2018) – a metamorphic event at this time is likely associated with magma underplating the Opinaca or a failed rifting event.
- 2666 – 2636 Ma Leucosome zircon age (Morfin et al., 2013) – Leucosome zircon ages are interpreted to indicate two metamorphic peaks, and possibly continuous metamorphism during their interval, within the Opinaca.
- 2652 Ma Metamorphic monazite from paragneiss, this study – a metamorphic event is interpreted at this time from four samples providing Concordia ages that are within error. This is the likely timing of convergent deformation and crustal thickening.
- 2636 Ma Metamorphic monazite and zircon from paragneiss, this study – a second metamorphic event is interpreted at this time from one samples providing monazite and zircon Concordia ages that are within error. This may be a second crustal thickening event associated with the onset of E-W convergence in the Lac Joubert region of the eastern La Grande.
- 2625 Ma Sheared pegmatite, this study – dextral deformation in regional shear zones was contemporaneous or post-dates this age.
- 2618 Ma Granite du Vieux-Comptoir (Goutier et al., 1999b) – undeformed granites of this suite are found within the Opinaca, and this date constrains the end of bulk, regional deformation (folding and penetrative strain).
- 2614 Ma Pegmatite (Bogatu, 2017) – Locally deformed pegmatite in a discrete dextral shear zone along the north boundary of the Opinaca and La Grande post-dates this age.

This sequence of events includes multiple different intervals of convergent deformation, punctuated with one extensional event. These events started during, and continued until up to 100 m.y. after, the emplacement of Duncan TTG intrusions. Subsequent intrusive suites are largely related to anataxis. This sequence is not consistent with sequential arc accretion models of Superior Province formation, considering the long and complex tectonic history that follows emplacement of Duncan intrusions, which would be the presumed arc. This sequence supports models of Superior Province formation that involve large-scale disaggregation followed by disorganized collision and imbrication of large crustal blocks and sliver, which could allow for rapid or localized transitions between extensional and compressional settings. The cascade of crustal blocks away from the central upwelling zone, the likely epicentre being the Minto block, provides an impetus for syn-magmatic tectonism in the La Grande, a period or localization of extension to create basins like the Opinaca, and a prolonged timeline to continue deformation events through the La Grande overriding the Opinaca, up to 50-70 m.y. after the cessation of Duncan magmatism.

8. Conclusions

In conclusion, the structure of the boundary region between the northern Opinaca and the La Grande subprovinces was defined by multiple deformation and metamorphic events that spanned at least 100 m.y., from ca. 2725 – 2610 Ma. An early, previously unidentified phase of convergent deformation occurred during or shortly after the intrusion of the ca. 2720-2705 Ma Duncan plutonic suite, and likely prior to the final deposition of Opinaca sediments. Deformation from this event created megascopic shear-related fold structures and north-dipping shear zones that accommodated thrust-sense, north-over-south motion.

Metamorphic conditions capable of producing monazite were attained ca. 2700 Ma. A subsequent episode of convergence likely affected the entire region, post-deposition of the Opinaca, and is likely associated with crustal thickening and the crystallization of metamorphic monazite in the Lac Joubert region ca. 2650 Ma. A second episode of monazite and metamorphic zircon crystallization ca. 2635 Ma may be associated with the onset of strike-slip tectonics, and localized E-W convergence in the eastern La Grande. Strike-slip motion became more localized into discrete shear zones by ca. 2625 Ma in the eastern La Grande. Metamorphic conditions and deformation may have persisted as late as 2600 Ma.

References

ALSOP, G.I. – HOLDSWORTH, R.E., 2006 – Sheath folds as discriminators of bulk strain type. Journal of Structural Geology, 28 (9), pages 1588-1606.

ALSOP, G.I. – HOLDSWORTH, R.E. – MCCAFFREY, K.J.W., 2007 – Scale invariant sheath folds in salt, sediments and shear zones. Journal of Structural Geology, 29 (10), pages 1585-1604.

AUCOIN, M. – BEAUDOIN, G. – CREASER, R. A. – ARCHER, P. – HANLEY, J., 2012 – Metallogeny of the Marco zone, Corvet Est, disseminated gold deposit, Baie-James, Quebec, Canada. Canadian Journal of Earth Sciences, 49 (10), pages 1154–1176.

AUGLAND, L. – DAVID, J. – PILOTE, P. – LECLERC, F. – GOUTIER, J. – HAMMOUCHE, H. – LAFRANCE, I. – TALLA TAKAM, F. – DESCHENES, P. – GUEMACHE, M., 2016 – Datations U-Pb dans les provinces de Churchill et du Superieur effectuees au GEOTOP en 2012-2013. Report RP 2015-01, Ministère des Ressources naturelles du Québec.

BANDYAYERA, D. – BURNIAUX, P. – MORFIN, S., 2011 – Geology of the Lac Brune (33G07) and Baie Gavaudan region (33G10). Report RP 2011-01 (A), Ministère des Ressources naturelles du Québec.

BANDYAYERA, D. – GOUTIER, J. – BURNIAUX, P., 2014 – Géochimie des roches volcaniques et intrusives de la région des lacs Guyer et Nochet, Baie-James. Report RP-2014-03, Ministère des Ressources naturelles du Québec.

BANDYAYERA, D. – RHÉAUME, P. – MAURICE, C. – BÉDARD, E. – MORFIN, S. – SAWYER, E. W. 2010 – Synthèse géologique du secteur du Réservoir Opinaca, Baie-James. Report RG 2010-02, Ministère des Ressources naturelles du Québec.

BÉDARD, J.H. – BROUILLETTE, P. – MADORE, L. – BERCLAZ, A., 2003 – Archaean cratonization and deformation in the northern Superior Province, Canada: an evaluation of plate tectonic versus vertical tectonic models. Precambrian Research, 127 (1-3), pages 61-87.

BÉDARD, J.H. – HARRIS, L.B., 2014 – Neoarchean disaggregation and reassembly of the Superior craton. Geology, 42 (11), pages 951-954.

BENN, K. – MILES, W. – GHASSEMI, M.R. – GILLETT, J., 1994 – Crustal structure and kinematic framework of the northwestern Pontiac Subprovince, Quebec: an integrated structural and geophysical study. Canadian Journal of Earth Sciences, 31 (2), pages 271-281.

BOGATU, A., 2017 – The Orfée prospect: a Neoarchean orogenic gold occurrence along the contact between the La Grande and Opinaca subprovinces (Eeyou Istchee James Bay, Québec). Masters thesis, Université Laval, Québec, Canada, 205 pages.

BUCHAN, K.L. – GOUTIER, J. – HAMILTON, M.A. – ERNST, R.E. – MATTHEWS, W.A., 2007 – Paleomagnetism, U–Pb geochronology, and geochemistry of Lac Esprit and other dyke swarms, James Bay area, Quebec, and implications for Paleoproterozoic deformation of the Superior Province. Canadian Journal of Earth Sciences, 44 (5), pages 643-664.

CADÉRON, S., 2003 – Interprétation tectonometamorphique du nord de la province du Supérieur, Québec, Canada. PhD thesis, Université du Québec à Montréal, Montréal, and Université du Québec à Chicoutimi, Canada; 314 pages.

CALVERT, A. – SAWYER, E. – DAVIS, W. – LUDDEN, J., 1995 – Archean subduction inferred from seismic images of a mantle suture in the Superior Province. Nature, 375 (6533), pages 670–674.

CARD, K., 1990 – A review of the Superior Province of the Canadian Shield, a product of Archean accretion. Precambrian Research, 48 (1), pages 99–156.

CARD, K. – POULSEN, K., 1998 – Geology and mineral deposits of the Superior Province of the Canadian Shield. Geology of the Precambrian Superior and Grenville Provinces and Precambrian Fossils in North America, Geological Survey of Canada, Geology of Canada, 7, 13–194.

CARRERAS, J. – DRUGUET, E. – GRIERA, A., 2005 – Shear zone-related folds. Journal of Structural Geology, 27 (7), pages 1229-1251.

CIESIELSKI, A., 1991 – Geology of the eastern Superior Province, James Bay and Bienville subprovinces. Geological Survey of Canada, open file 2398, 9 pages.

CLEVEN, N. – HARRIS, L. – GUILMETTE, C., 2019 (in press) – Structural interpretation of enhanced high-resolution aeromagnetic depth slices of the Eeyou Istchee Baie-James region, Québec Superior province. Ministère des ressources naturelles, Québec, Report MB, 82 pages.

CLEVEN, N. – GUILMETTE, C. – CÔTÉ-ROBERGE, M. – DAVIS, D.W. – GOUTIER, J. – (in prep.) Detrital zircon geochronology of the Opinaca and La Grande subprovinces, northern Superior Craton: Constraints on the geodynamic significance of Archean metasedimentary belts.

CORFU, F. – STOTT, G.M. – BREAKS, F.W., 1995 – U-Pb geochronology and evolution of the English River Subprovince, an Archean low P-high T metasedimentary belt in the Superior Province. Tectonics, 14 (5), pages 1220-1233.

CÔTÉ-ROBERGE, M., 2018 – Contexte tectonométamorphique du nord-ouest du complexe de Laguiche, sous-province d'Opinaca, Eeyou Itschee Baie-James. Masters thesis, Université Laval, Québec, Canada; 201 pp.

CÔTÉ-ROBERGE, M. – GUILMETTE, C. – GOUTIER, J., 2016 – Étude du contexte tectono-métamorphique du Complexe de Laguiche, Sous-province d'Opinaca, Eeyou Istchee Baie-James, Québec. Ministère des ressources naturelles, Québec, Report MB 2016-13, 27 pp.

DAVIS, D. W., 2002 – U–Pb geochronology of Archean metasedimentary rocks in the Pontiac and Abitibi subprovinces, Quebec, constraints on timing, provenance and regional tectonics. Precambrian Research, 115 (1), 97-117.

DAVIS, D.W. – SIMARD, M. – HAMMOUCHE, H. – BANDYAYERA, D. – GOUTIER, J. – PILOTE, P. – LECLERC, F. – DION, C., 2014 – Datations U-Pb dans les provinces du Supérieur et de Churchill en 2011-2012. Ministère de l'Énergie et des Ressources naturelles, Québec; RP 2014-05, 62 pages.

DUPARC, Q. – DARE, S. A. – COUSINEAU, P. A. – GOUTIER, J., 2016 – Magnetite chemistry as a provenance indicator in Archean metamorphosed sedimentary rocks. Journal of Sedimentary Research, 86 (5), pages 542-563.

FONTAINE, A. – DUBÉ, B. – MALO, M. – MCNICOLL, V. – BRISSON, T. – DOUCET, D. – GOUTIER, J., 2015 – Geology of the metamorphosed Roberto gold deposit (Éléonore Mine), Baie-James region, Québec: diversity of mineralization styles in a polyphase tectono-metamorphic setting. *In:* Targeted Geoscience Initiative 4: Contributions to the Understanding of Precambrian Lode Gold Deposits and Implications for Exploration, Editors: B. Dubé and P. Mercier-Langevin, Geological Survey of Canada, Open File 7852, pages 209–225.

GAUTHIER, M. – TRÉPANIER, S. – GARDOLL, S., 2007 – Metamorphic gradient: a Regional-Scale Area Selection Criterion for Gold in the Northeastern Superior Province, Eastern Canadian Shield. Society of Economic Geologists Newsletter, 69, pages 10-15.

GOUTIER, J. – DOUCET, P. – DION, C. – BEAUSOLEIL, C. – DAVID, J. – PARENT, M. – DION, D.-J., 1998 – Géologie de la région du lac Kowskatehkakmow (33F/06). Ministère des Ressources naturelles, Québec, RG 98-16, 48 pages, 1 map.

GOUTIER, J. – DION, C. – DAVID., J. – DION, D.-J., 1999a – Géologie de la région de la passe Shimusuminu et du lac Vion (33F/11 et 33F/12). Ministère des Ressources naturelles, Québec, RG 98-17, 41 pages, 2 maps.

GOUTIER, J. – DION, C. – LAFRANCE, I. – DAVID, J. – PARENT, M. – DION, D., 1999b – Géologie de la région des lacs Langelier et Threefold (SNRC 33F/03 et 33F/04). Ministère des Ressources naturelles et de la Faune, Québec, RG 98-18, 52 pages, 2 maps.

GOUTIER, J. – DION, C. – OUELLET, M.-C. – DAVID, J. – PARENT, M., 2000 – Géologie de la région des lacs Guillaumat et Sakami (SRNC 33F/02 et 33F/07). Report, Ministère des Ressources naturelles du Québec, RG 99-15, 37 pages.

GOUTIER, J. – DION, C. – OUELLET, M.-C. – DAVIS, D. W. –DAVID, J. – PARENT, M., 2002 – Géologie de la région du lac Guyer (33G/05, 33G/06 et 33G/11). Ministère des Ressources naturelles du Québec, RG 2001-15, 53 pages, 3 maps.

GOUTIER, J. – DION, C. – OUELLET, M.-C. – MERCIER-LANGEVIN, P. – DAVIS, D. W., 2001 – Géologie de la Colline Masson, de la passe Awapakamich, de la Baie Carbillet et de la passe Pikwahipanan (SRNC 33F/09, 33F/10, 33F/15 et 33F/16). Ministère des Ressources naturelles du Québec, RG 2000-10, 69 pages, 4 maps.

HARRIS, L.B. – BÉDARD, J.H., 2014 – Crustal evolution and deformation in a non-plate-tectonic Archaean Earth: Comparisons with Venus. *In*: Evolution of Archean Crust and Early Life. Editors: Y Dilek and H. Furnes; Modern Approaches in Solid Earth Sciences, volume 7, Springer, Dordrecht, pages 215-291.

HARRIS, N.B.W. – GOODWIN, A.M., 1976 – Archean rocks from the eastern Lac Seul region of the English River Gneiss Belt, northwestern Ontario, part 1. Petrology, chemistry, and metamorphism. Canadian Journal of Earth Sciences, 13 (9), pages 1201-1211.

HOULÉ, M.G. – GOUTIER, J. – SAPPIN, A.-A. –MCNICOLL, V.J., 2015 – Regional characterization of ultramafic to mafic intrusions in the La Grande Riviére and Eastmain domains, Superior Province, Quebec. Targeted Geoscience Initiative 4: Canadian nickel-copper-platinum group elements-chromium ore systems – fertility, pathfinders, new and revised models, Geological Survey of Canada, Geology of Canada, pages 125–137.

JAFFEY, A.H. – FLYNN, K.F. – GLENDENIN, L.E. – BENTLEY, W.C. – ESSLING, A.M., 1971 – Precision measurement of half-lives and specific activities of 235U and 238U. Physical Review 4, 1889-1906.

JIANG, D., 2014 – Structural geology meets micromechanics: A self-consistent model for the multiscale deformation and fabric development in Earth's ductile lithosphere. Journal of Structural Geology, 68, pages 247-272.

KERRICH, R. – FENG, R., 1992 – Archean geodynamics and the Abitibi-Pontiac collision: implications for advection of fluids at transpressive collisional boundaries and the origin of giant quartz vein systems. Earth-Science Reviews, 32 (1-2), pages 33-60.

KEHLENBECK, M. M., 1976 – Nature of the Quetico–Wabigoon boundary in the de Courcey–Smiley Lakes area, northwestern Ontario. Canadian Journal of Earth Sciences, 13 (6), pages 737-748.

LAMOTHE, D. – THÉRIAULT, R. – LECLAIR, A., 2000 – Géologie de la région du Lac Nitchequon. Ministère des ressources naturelles, Québec, Report RG 99-14, 46 pp.

LUDWIG, K.R., 1998 – On the treatment of concordant uranium-lead ages. Geochimica et Cosmochimica Acta, 62, 665-676.

LUDWIG, K.R., 2003 – User's manual for Isoplot 3.00 a geochronological toolkit for Excel. Berkeley Geochronological Center Special Publication, 4, 71 p.

MERCIER-LANGEVIN, P. – DAIGNEAULT, R. – GOUTIER, J. – DION, C. – ARCHER, P., 2012 – Geology of the Archean Intrusion-Hosted La-Grande-Sud Au-Cu Prospect, La Grande Subprovince, Eeyou Istchee James Bay region, Québec. Economic Geology, 107 (5), pages 935–962.

MILLER, H.G. – SINGH, V., 1994 – Potential field tilt – A new concept for location of potential field sources. Journal of Applied Geophysics, 32 (2-3), pages 213-217.

MORFIN, S. – SAWYER, E. W. – BANDYAYERA, D., 2013 – Large volumes of anatectic melt retained in granulite facies migmatites: An injection complex in northern Quebec. Lithos, 168, pages 200-218.

MOSER, D.E. – HEAMAN, L.M. – KROGH, T.E. – HANES, J.A., 1996 – Intracrustal extension of an Archean orogen revealed using single-grain U-Pb zircon geochronology. Tectonics, 15 (5), pages 1093-1109.

MOUGE, P. – ASTIC, T., 2013 – rapport logistique et technique, leve magnetique heliporte, projets eleonore regional, lac Menarik et lac La Grande est. Mines Virginia Inc. Assessment work submitted to the Government of Québec. GM 68056, 34 pages and 9 maps.

PERCIVAL, J. A., 1989 – A regional perspective of the Quetico metasedimentary belt, Superior Province, Canada. Canadian Journal of Earth Sciences, 26 (4), pages 677-693.

PERCIVAL, J. A. – SKULSKI, T. – SANBORN-BARRIE, M. – STOTT, G. M. – LECLAIR, A. D. – CORKERY, M. T. – BOILY, M., 2012 – Geology and tectonic evolution of the Superior Province, Canada. In Tectonic Styles in Canada: The Lithoprobe Perspective, Geological Association of Canada Special Paper, 49, pages 321–378.

POLAT, A. – KERRICH, R. – WYMAN, D.A., 1998 – The late Archean Schreiber–Hemlo and White River–Dayohessarah greenstone belts, Superior Province: collages of oceanic plateaus, oceanic arcs, and subduction–accretion complexes. Tectonophysics, 289 (4), pages 295-326.

PIETTE-LAUZIÈRE, N. – GUILMETTE, C. – BOUVIER, A. – PERROUTY, S. – PILOTE, P. – GAILLARD, N. – LYPACZEWSKI, P. – LINNEN, R.L. – OLIVO, G.R., 2019 – The timing of prograde metamorphism in the Pontiac Subprovince, Superior craton; implications for Archean geodynamics and gold mineralization. Precambrian Research, 320, pages 111-136.

RAVENELLE, J. F. – DUBÉ, B. – MALO, M. – MCNICOLL, V. – NADEAU, L. – SIMONEAU, J., 2010 – Insights on the geology of the world-class Roberto gold deposit, Éléonore property, Baie-James area, Quebec. Geological Survey of Canada, Current Research 2010-1, 26 pp.

SALEM, A. – WILLIAMS, S. – FAIRHEAD, D. – SMITH, R. – RAVAT, D., 2007 – Interpretation of magnetic data using tilt-angle derivatives. Geophysics, 78 (1), pages 1-10.

SIGÉOM, 2018: Système d'information géominière du Québec, carte interactive. Ministère des Ressources naturelles du Québec, http://sigeom.mines.gouv.qc.ca.

SIMARD, M. – PARENT, M. – DAVID, J. – SHARMA, K.N.M., 2003 – Géologie de la région de la rivière Innuksuac (34K et 34 L). Ministère des Ressources naturelles, Québec, RG 2002-10, 43 pp.

STOTT, G.M. – CORKERY, M.T. – PERCIVAL, J.A. – SIMARD, M. – GOUTIER, J., 2010 – A revised terrane subdivision of the Superior Province. Ontario Geological Survey, Open File Report, 6260, pages 20-1.

TOMLINSON, K.Y. – DAVIS, D.W. – STONE, D. – HART, T.R., 2003 – U-Pb age and Nd isotopic evidence for crustal recycling and Archean terrane development in the south-central Wabigoon subprovince, Canada. Contributions to Mineralogy and Petrology, 144, pages 684-702.

Figures

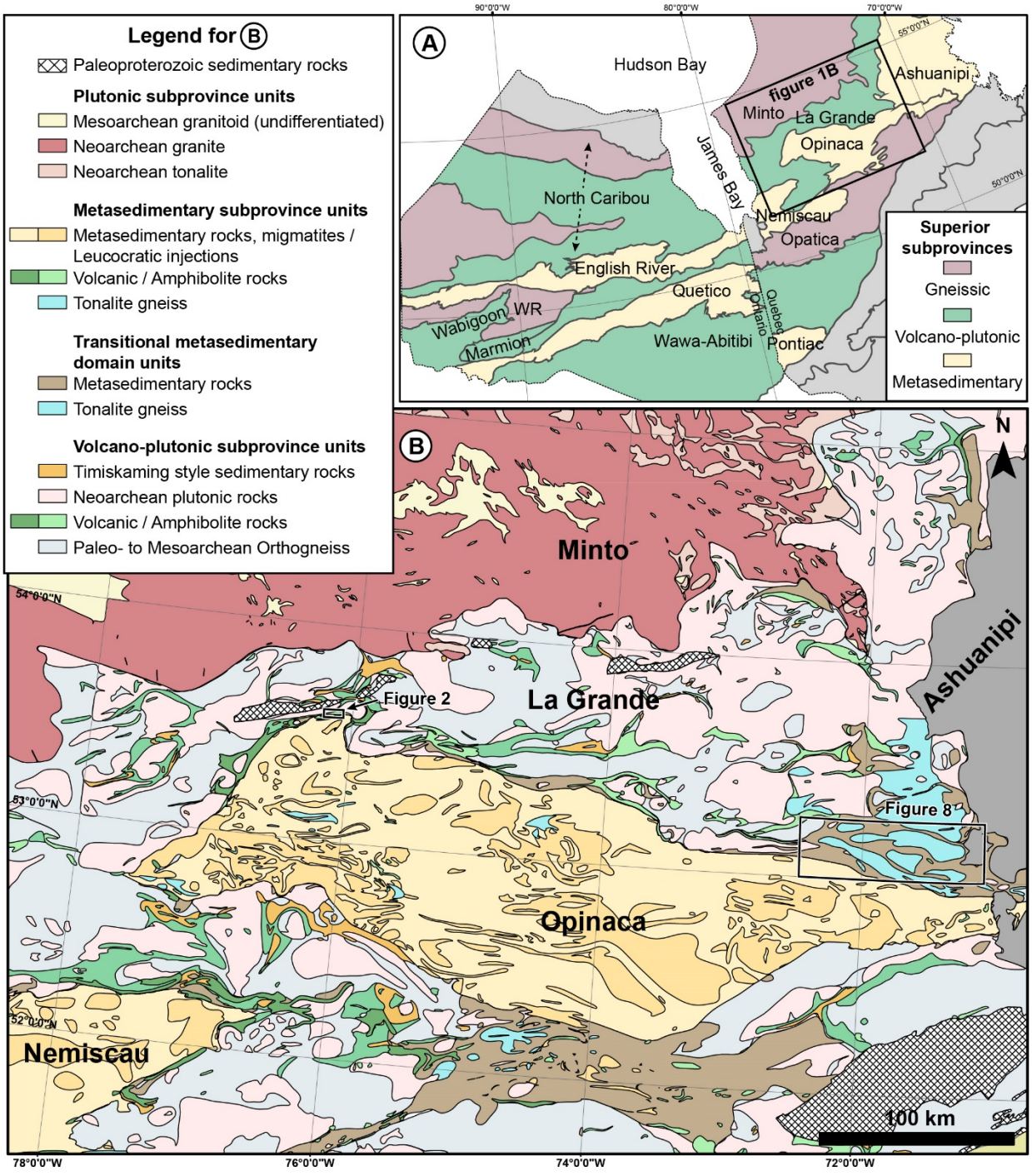

Figure 1: A) Map of Superior Province subprovinces based on Stott et al. (2010). The field area, indicated on the map, is in the Eeyou Istchee Baie-James region. B) Tectonostratigraphic map of the Eeyou Istchee Baie-James region, centred on the Opinaca and La Grande subprovinces. Locations of the Lac Sakami and Lac Joubert study areas are indicated as boxes for Figures 2 and 8, respectively. Figure 2 is a small box at the northern tip of the Opinaca.

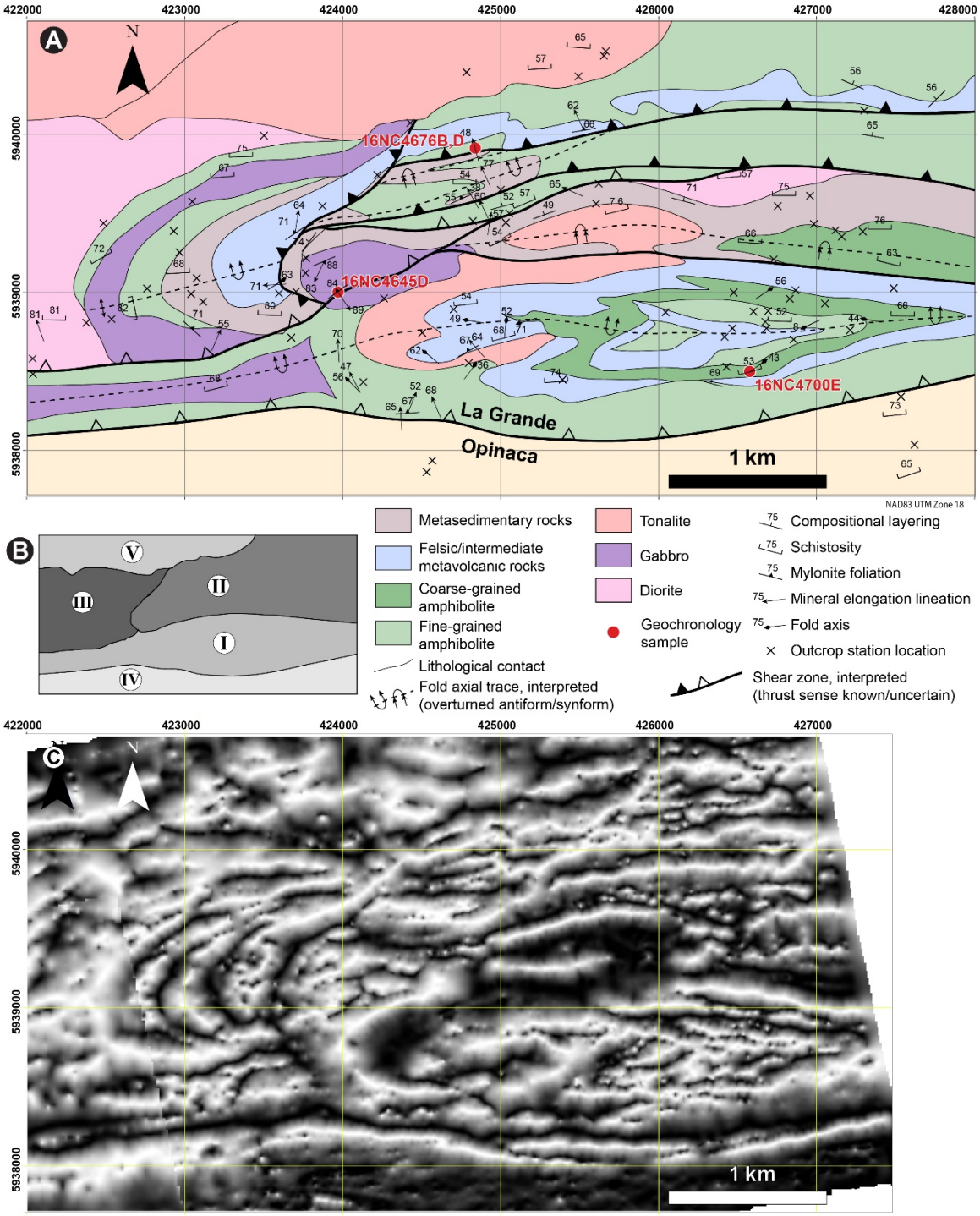

Figure 2: A) Geological map of the Lac Sakami region study area showing sample locations. The inferred boundary between the Opinaca and La Grande subprovinces is indicated. B) Structural domains interpreted from the geologic map in A). Major shear zones define most domain boundaries, separating rock units with different degrees and styles of deformation. The labels I-V are referred to in the text. C) Tilt-angle derivative image (Miller and Singh, 1994; Salem et al., 2007; Cleven et al., 2019) of a high-resolution aeromagnetic survey data of the map area from A). The source of the aeromagnetic data is Mouge and Astic (2013). Major structural features including large-scale folds in domains I and III are apparent in the image. Major boundaries, such as between the La Grande and Opinaca, are pronounced, and are interpreted to represent major ductile thrusts.

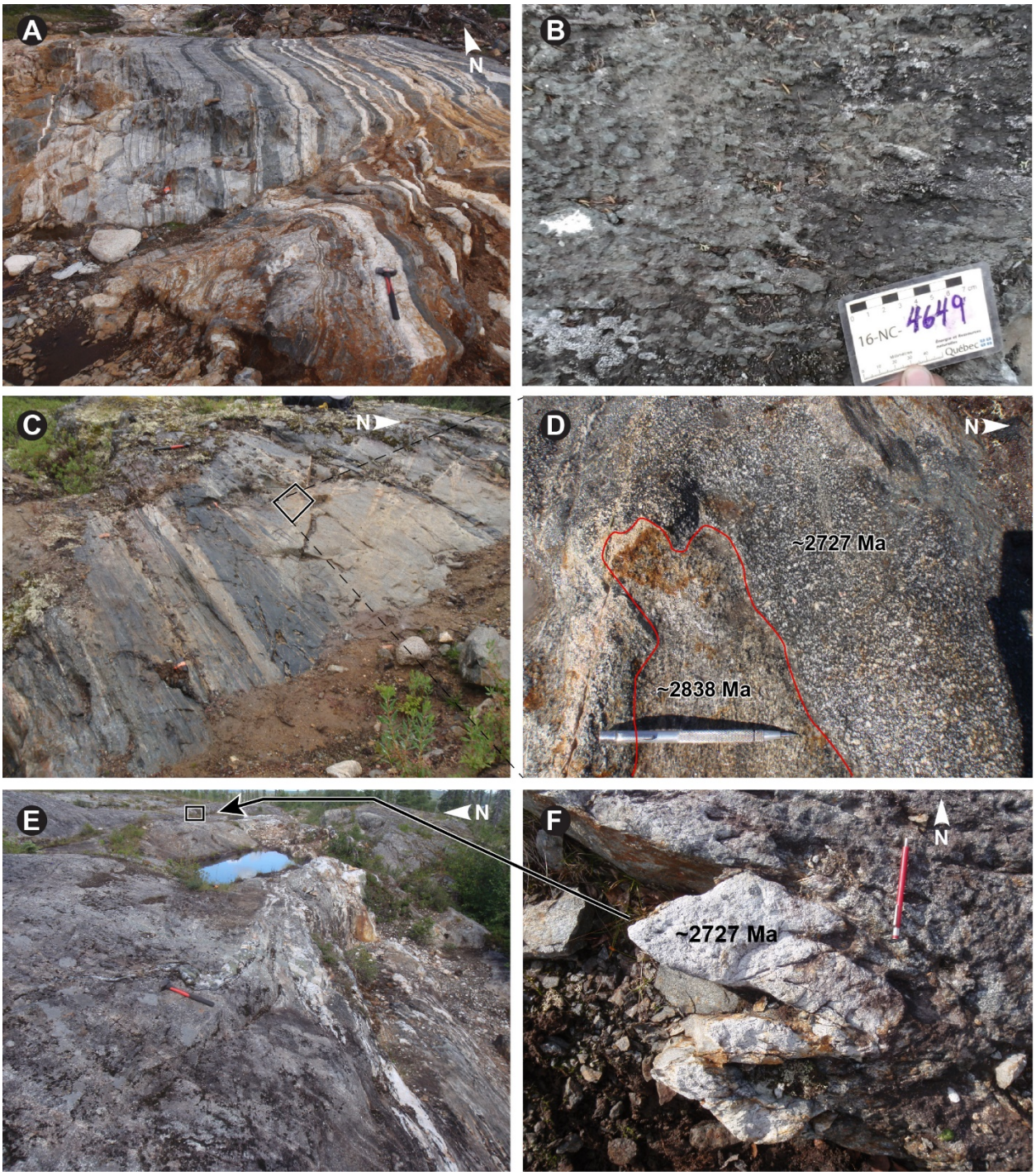

Figure 3: *caption on next page*

Figure 3 (previous page): Field photos of lithologic, metamorphic and structural features in the Lac Sakami field area. A) Interlayered volcanic and volcaniclastic horizons in structural domain III. B) Amphibole porphyroblasts aligned with the foliation in relief on a weathered surface of amphibolite in domain I. C) Well-foliated and locally sheared gabbro, amphibolite, and tonalite. One horizon of tonalite is crosscut by a weakly deformed quartz-feldspar porphyritic dyke within the indicated box. The crosscutting relationship is pictured in D). Located in domain II. D) Quartz-feldspar porphyritic dyke crosscutting well-foliated tonalite. Both lithologies were sampled for geochronology to constrain the timing of foliation development and shearing in domain II (samples 16NC4676B,D indicated in Figure 2A). E) Shear zone in gabbro at the boundary between domains I and II. Multiple generations of veins are hosted within the shear zones (white material in centre), some of which are mylonitized in the centre of the shear zone. Veins exhibit folds within the margins of the shear zone. F) A thin, folded tonalite dyke located in the margins of the shear zone depicted in E) (location indicated). The dyke crosscuts the shear zone foliation, is not mylonitized yet is folded, and was thus sampled for geochronology to establish the timing of late-stage deformation in the shear zone. This is sample 16NC4645D and its location is indicated on Figure 2A.

Figure 4 (next page): Field photos of structural features in the Lac Sakami field area. A) Disharmonic close to tight folds in compositionally interlayered volcanic rocks in structural domain I. B) Localized shearing in fine compositionally interlayered volcanic rocks resulting in zones of a transposed foliation that is parallel to the fold axial surface in domain III. C) Passive slip tight to isoclinal folds apparent in tonalite dykes intruded into amphibolite. Hammer for scale in upper left corner. D) Isoclinal folds in thinly banded material in amphibolite, located along the central fold axial trace in domain I. E) Mylonitic foliation in tonalite dipping moderately north in domain II. F) Mineral stretching lineation on mylonite foliation surface in domain II pitching steeply westward.

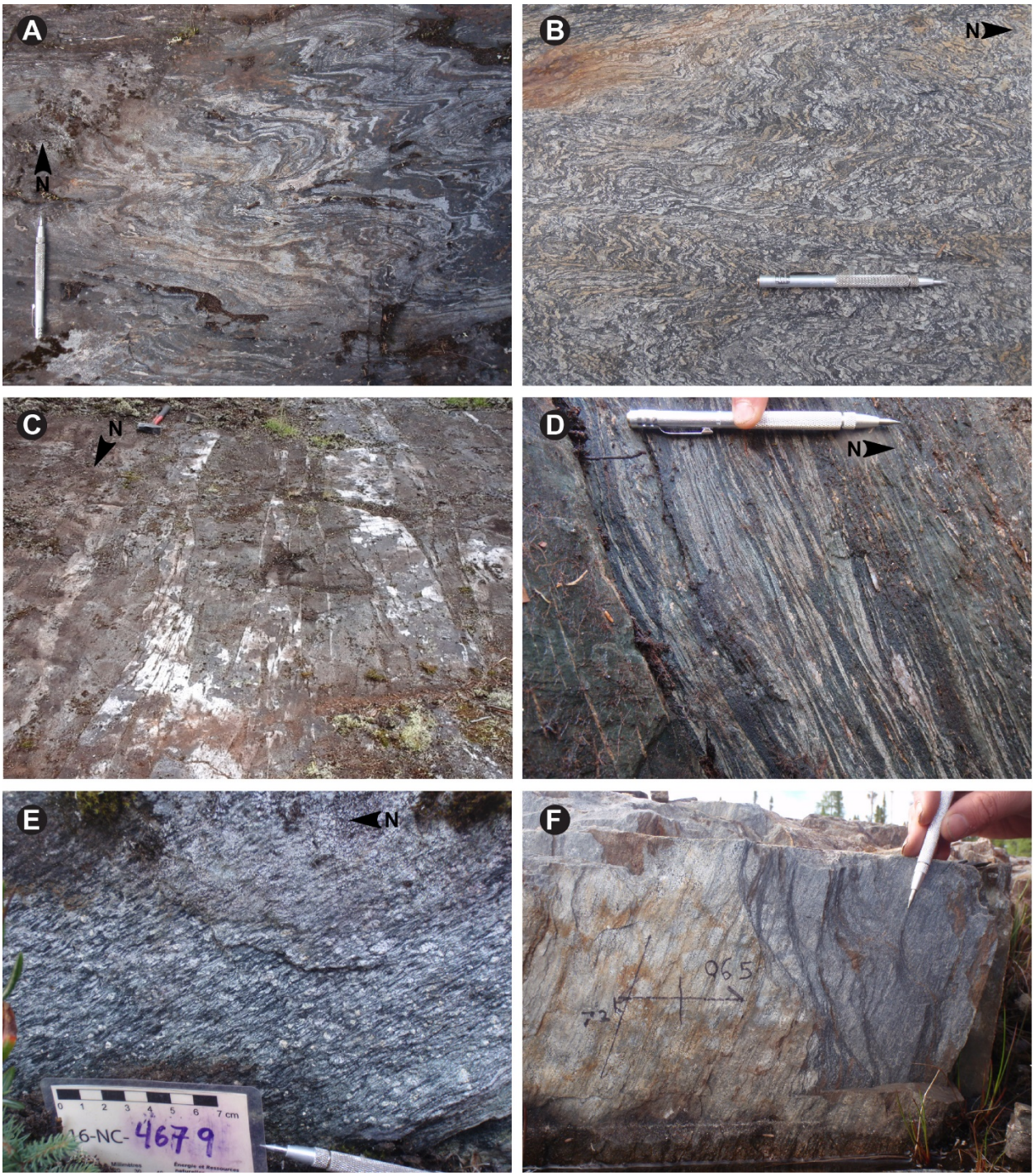

Figure 4: *caption on previous page.*

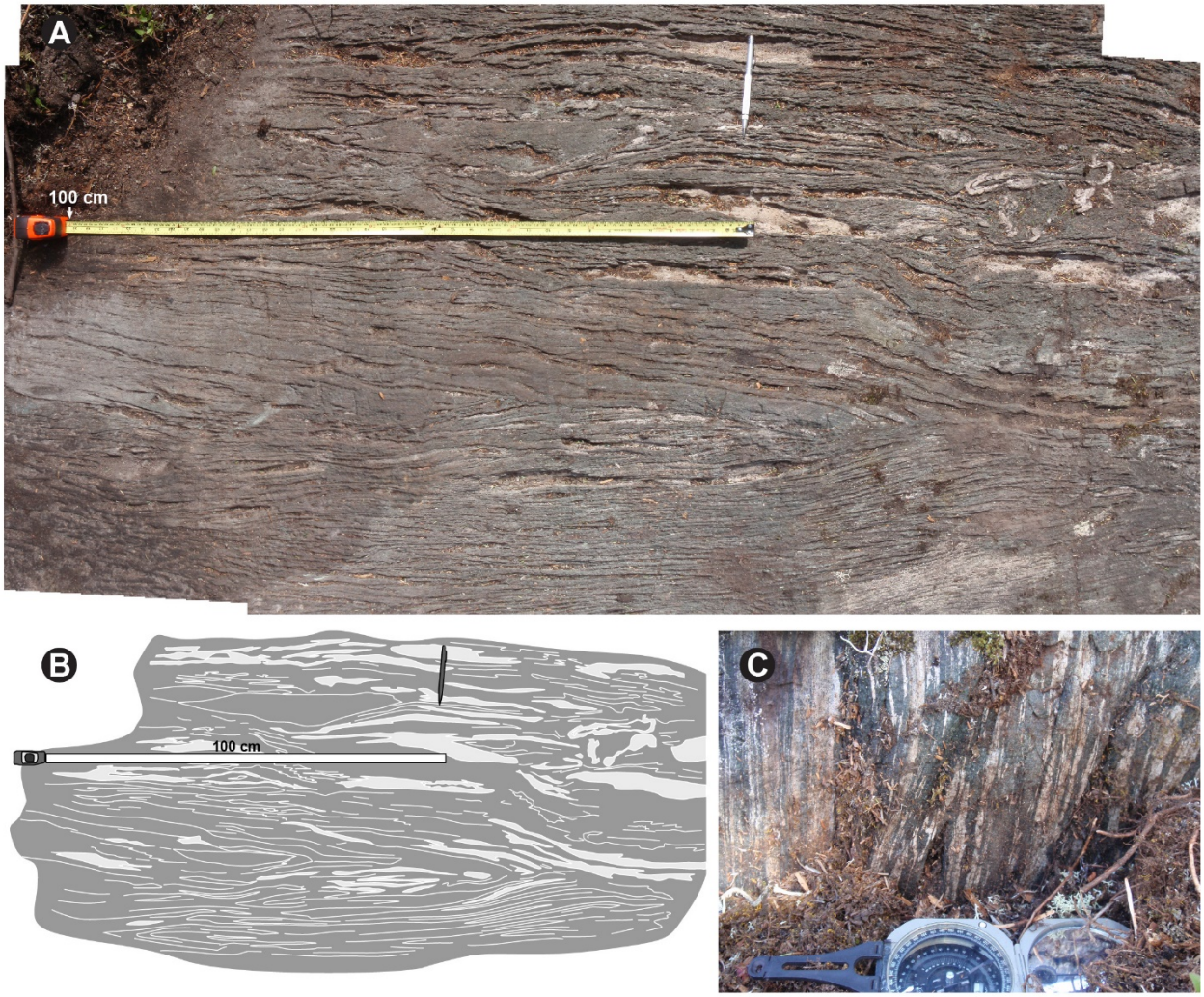

Figure 5: Field photos of a horizontal outcrop exhibiting shear-related folds in compositionally banded rocks in structural domain I. A) Stitched photo of tight to isoclinal folds made apparent by the differential erosion between mafic and felsic interbeds. Some fold structures are elliptical with closures at east and west ends, exhibit nested traces, are intrafolial, and have high aspect ratios. Such folds are consistent with doubly plunging or sheath folds associated with shearing. B) Schematic trace of the outcrop in A). C) The exposed vertical face of the outcrop in A) also exhibits isoclinally folded horizons.

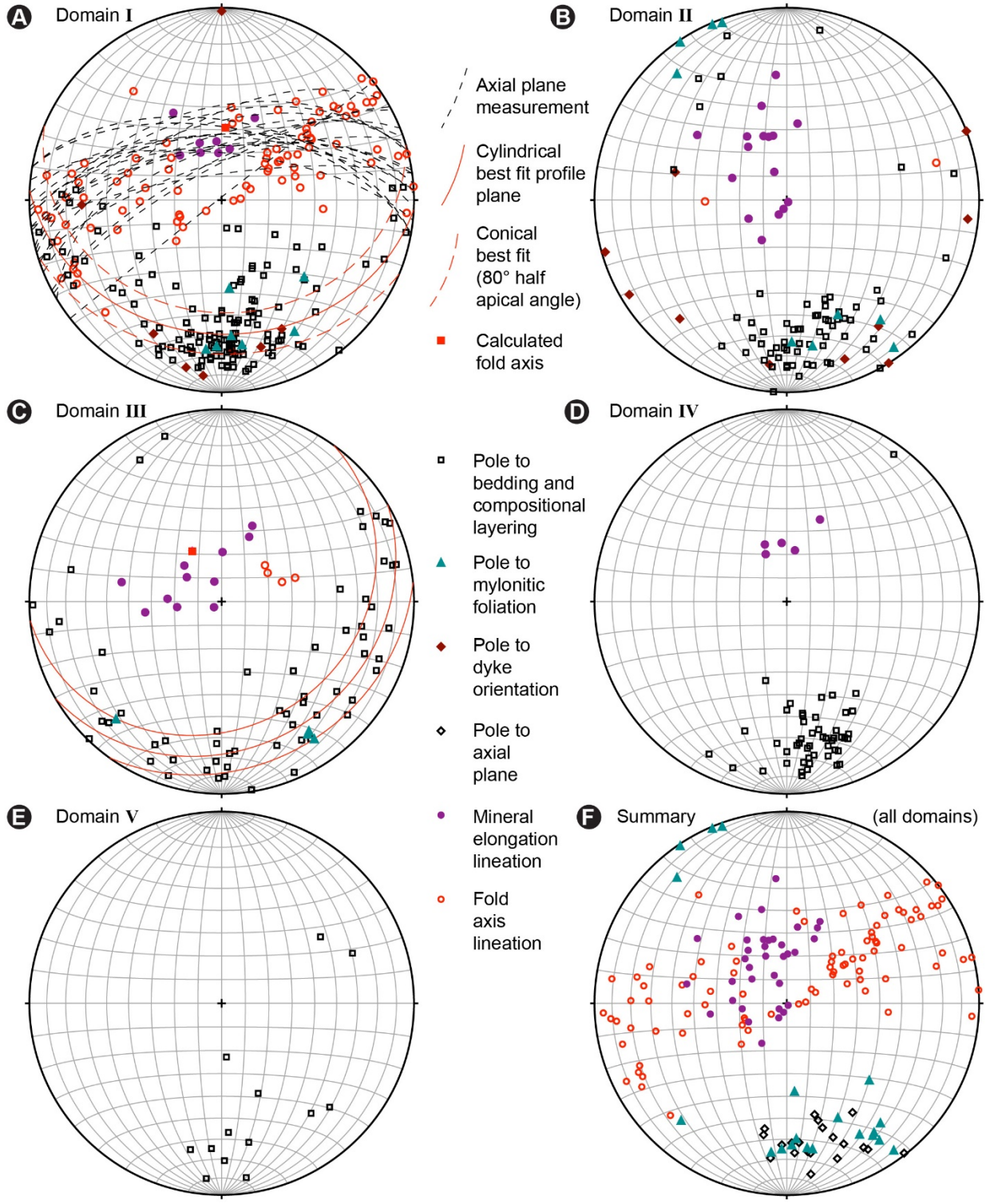

Figure 6: caption *on next page.*

Figure 6 (previous page): Stereonets of Lac Sakami region structural data. A) All domain I foliations dip moderately north and are generally parallel, including bedding and compositional layering measurements, and axial planes of folds. This is an indication that the map-scale fold is isoclinal and overturned. Outcrop scale fold axis measurements are common, and they exhibit a wide array of orientations spread throughout the extent of axial plane orientations. A slight concentration of fold axes plunges moderately northeast. B) Domain II foliations dip moderately northward, and mylonite foliations cluster parallel to bedding and compositional layering. Mineral elongation lineations are generally down dip on their respective foliation. C) The domain III map-scale fold is defined by an even spread of bedding and compositional layering poles along a shallowly southeast dipping profile plane. The steeply plunging calculated fold axis is roughly parallel to a small cluster of fold axis measurements. Mineral elongation lineations cluster around the axis as well, even though they are associated with shearing near the domain boundaries. The similarity between the spread of measurements in north and south limbs indicate that the fold is tight to isoclinal and overturned. D) Domain IV measurements, from within the Opinaca, cluster in an orientation dipping moderately to steeply north. Few lineation measurements are oriented down dip on their respective foliation. E) Limited measurements in domain V show that the foliations in Duncan intrusions are generally parallel to regional orientations. F) Summary stereonet of all lineations, mylonite and axial plane foliations from all domains. Notably, mylonite foliations are parallel to the axial planes of folds suggesting folds may have formed during shearing. Fold axis measurements, dominantly represented by domain I, are spread throughout the extent of axial plane orientations, and mineral elongation lineations are oriented down dip on the regional foliation, clustering at a moderately steep north-northwestward plunge.

Figure 7 (next page): Microstructural kinematic indicators. A) Altered feldspar σ-type porphyroclasts in sheared felsic meta-volcanic rock under cross polarized light. Tails of quartz grains form an asymmetric strain shadow that indicates a dextral sense of motion in the reference frame of the image. This correlates to a north-over-south sense of motion in the reference frame of the oriented sample. Quartz in the strain shadow exhibits polygonal grain shapes consistent with static recovery textures. B) Plagioclase σ-type porphyroclast in sheared felsic meta-volcanic rock under cross polarized light. Tails of quartz grains form asymmetric strain shadows that indicate a dextral sense of motion in the reference frame of the image. This correlates to a north-over-south sense of motion in the reference frame of the oriented sample. C) Mantled amphibole σ-type porphyroclasts in sheared amphibolite under plane polarized light. Tails of plagioclase, and the mantling foliation, form strain asymmetric shadows which indicate a sinistral sense of motion in the reference frame of the image. This correlates to a south-over-north sense of motion in the reference frame of the oriented sample.

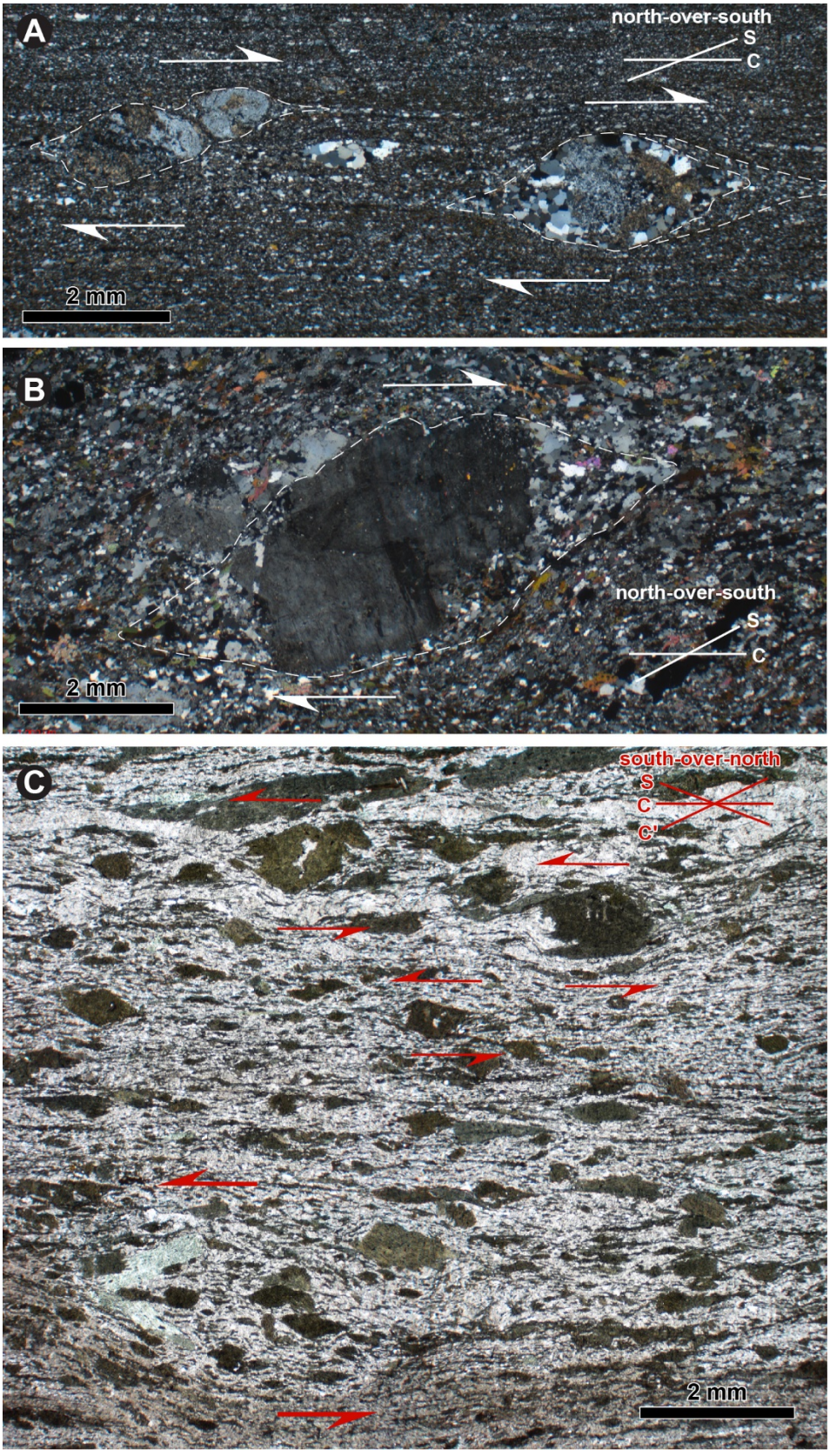

Figure 7: *caption on previous page.*

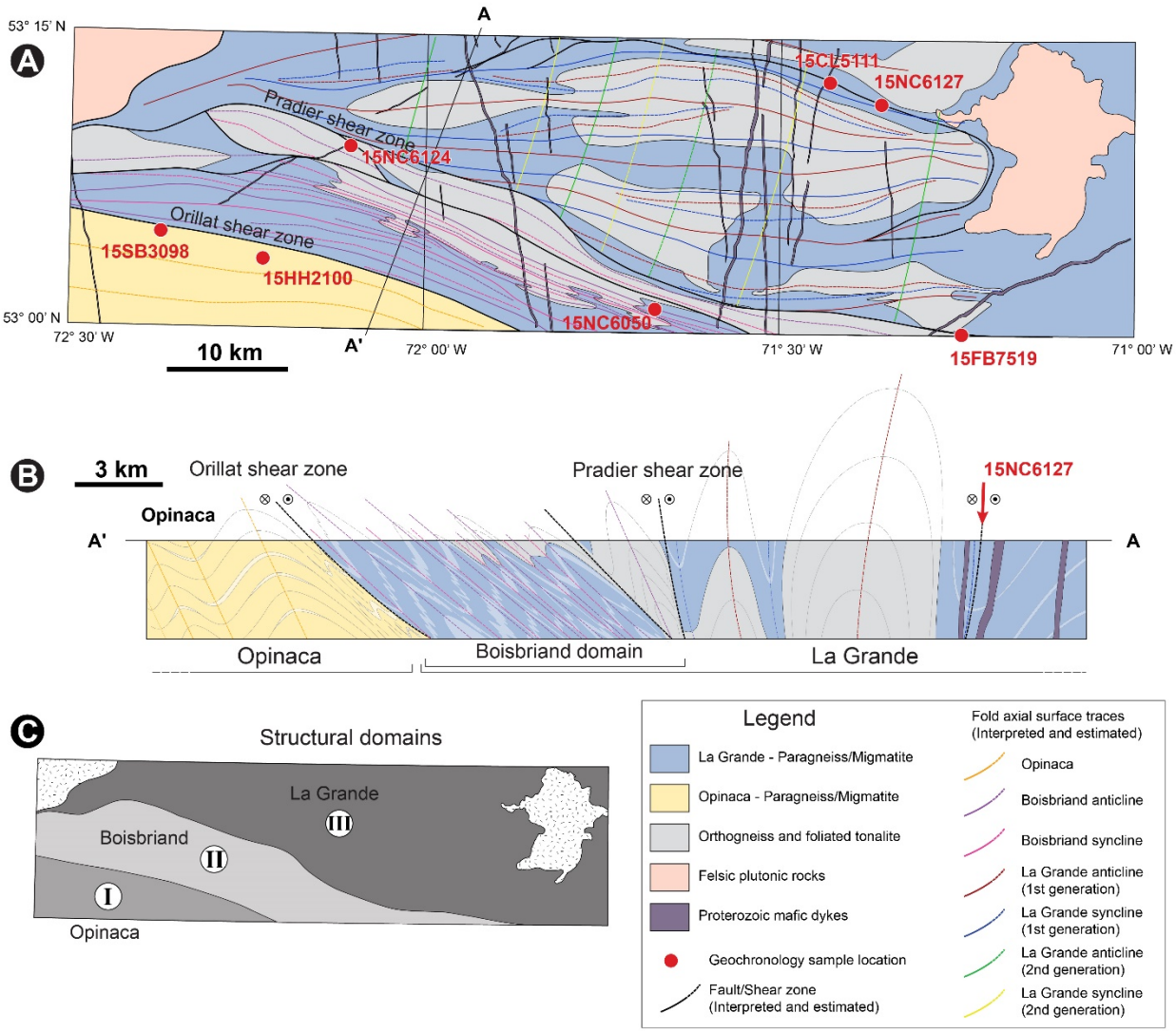

Figure 8: A) Simplified geological map of the Lac Joubert region showing general lithologies, fold-related structural interpretations and shear zones. Geochronology sample locations are indicated in red. B) Structural cross section along line A-A′, as indicated in A) (no vertical exaggeration). C) Structural domains interpreted from the geologic map in A).

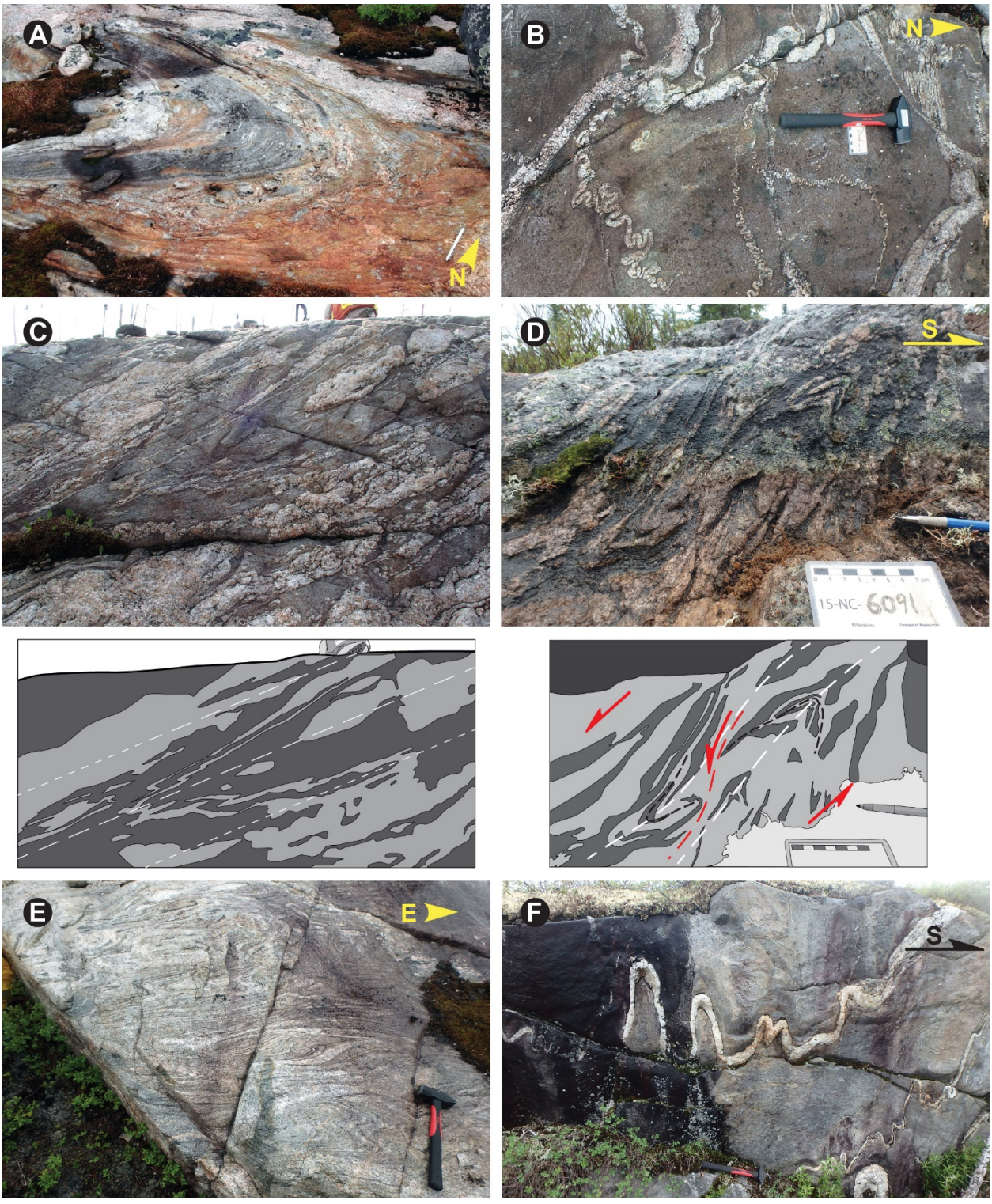

Figure 9: *caption on next page.*

Figure 9 (previous page): Field photos of folds in the Lac Joubert region. A) Open folds in paragneiss of the Opinaca (domain I). Pen in bottom right corner for scale. B) Ptygmatic folds of leucocratic injections in paragneiss of the Opinaca (domain I). C) Tight overturned folds of leucocratic injections in paragneiss viewed on vertical outcrop surface in the Boisbriand (domain II). Person on top of outcrop for scale. Schematic sketch of leucocratic injections (light gray) in paragneiss (dark gray) with annotated axial surface traces (white) below. D) Tight, overturned, progressively refolded folds of leucocratic injections in paragneiss viewed on vertical outcrop surface in the Boisbriand (domain II). Schematic sketch of leucocratic injections (light gray) in paragneiss (dark gray) with annotated 1^{st} generation axial surface traces (black) and 2^{nd} generation axial surface traces (white) below. E) Tight folds in orthogneiss of the La Grande (domain III) Joubert suite. F) Upright close folds in a leucocratic injection in paragneiss in the La Grande (domain III). Hammer at bottom centre for scale.

Figure 10 (next page): Field photos of shear zone structures in granulites and migmatites in the Lac Joubert region. A) Exceptionally straight, evenly spaced, stromatic migmatite layering with parallel thick leucocratic injections characterize much of the Pradier shear zone. B) Isoclinal folds of leucocratic injections in the Pradier shear zone exhibit a dextral sense of rotation in plan view yet appear as tight to isoclinal overturned folds on vertical surfaces. C) Vertical surface of the Orillat shear zone shows that exceptionally straight, evenly spaced, stromatic migmatite layering with parallel thick leucocratic injections (light gray in schematic drawing at right) in paragneiss (medium gray in schematic drawing) define the shear zone foliation. Rare σ-type structures of leucosome or leucocratic injection provide a dextral sense of shear for the shallowly north dipping shear zone (indicated in red on schematic drawing). D) Close-up view of quasi-mylonitic textures in sheared migmatites of the Orillat shear zone. Mantled σ-type structures of leucosome or leucocratic injection have asymmetric tails indicating a dextral sense of shear.

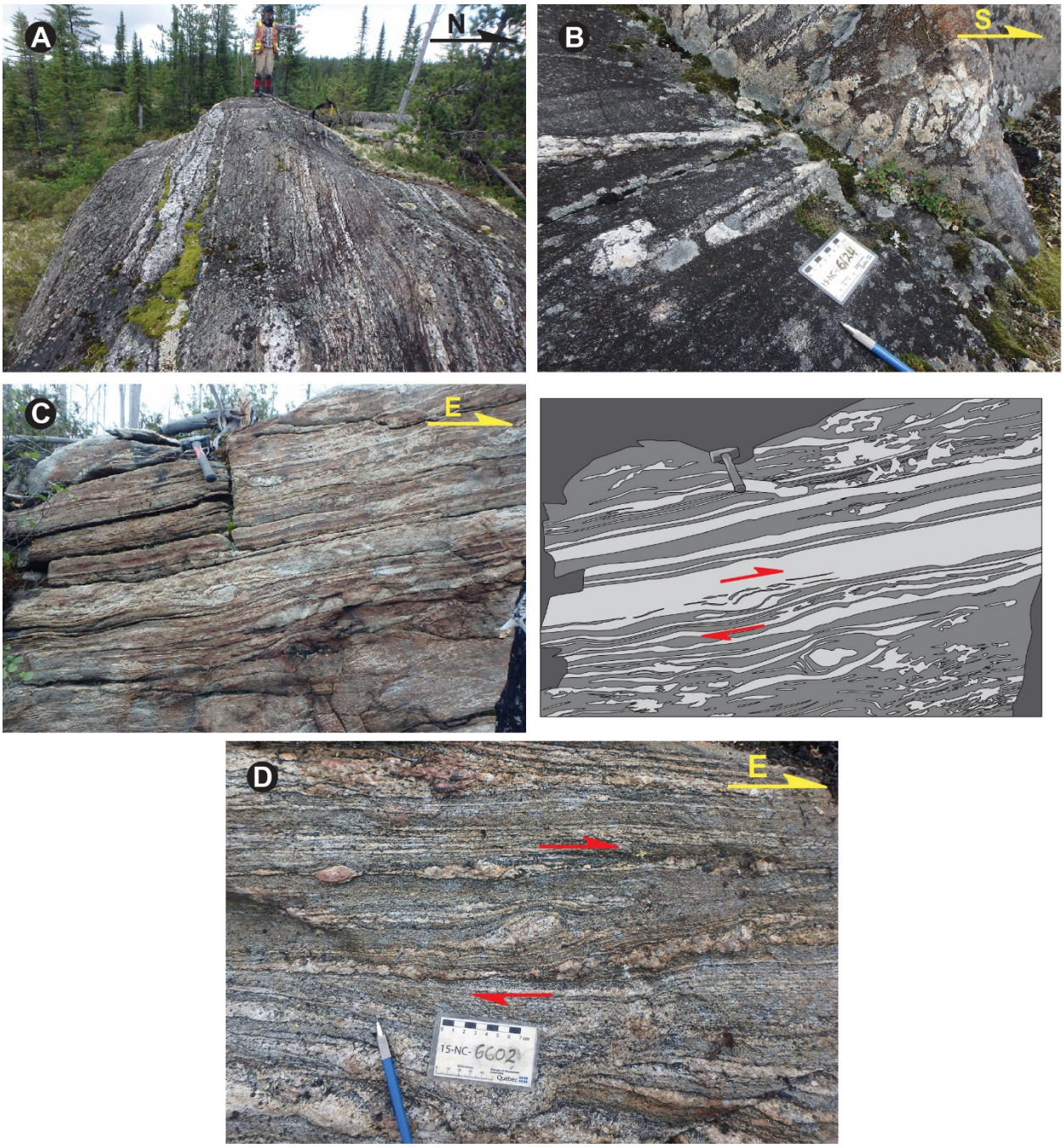

Figure 10: caption on previous page.

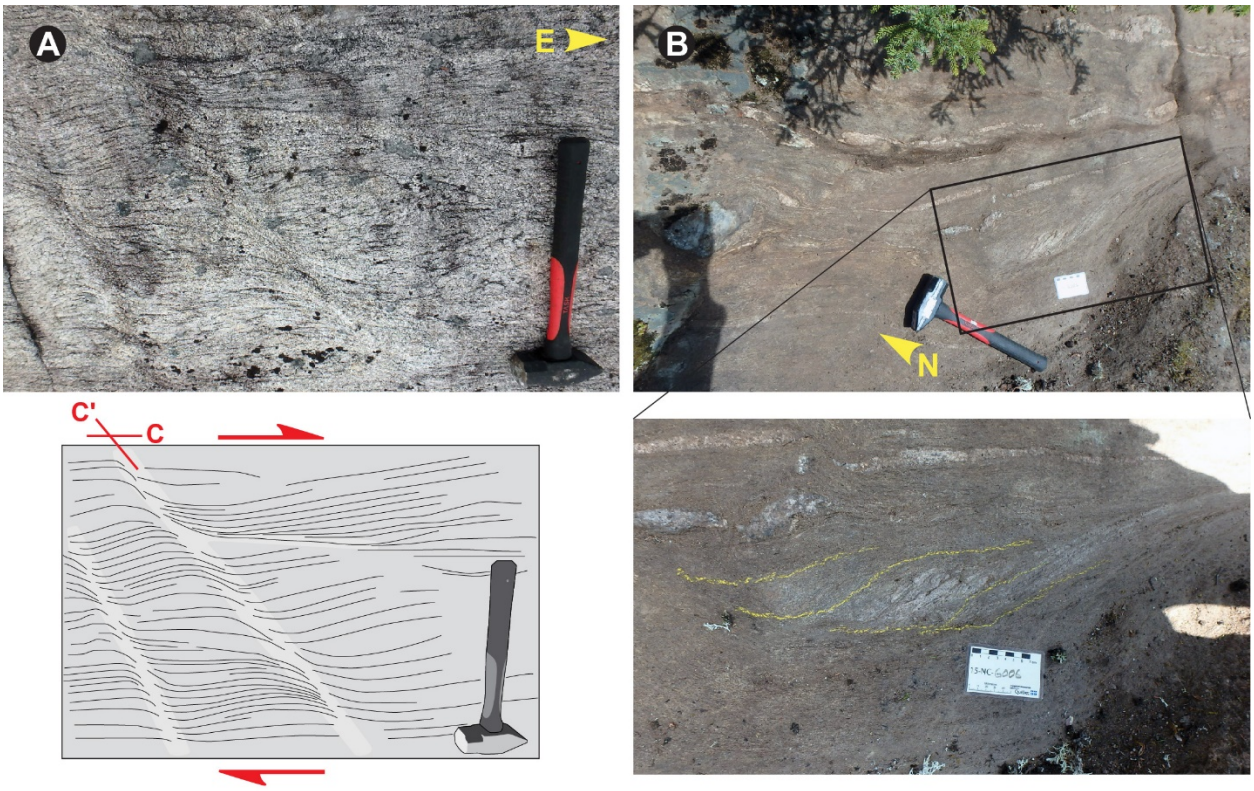

Figure 11: Field photos of shear structures in the La Grande (domain III). A) Orthogneiss units commonly exhibit localized deflection of the regional foliation in NW-SE oriented, regularly spaced outcrop-scale shear zones, similar to a C′ fabric associated with E-W shearing. Schematic diagram below. B) Rare N-S oriented, thin local shear zones are present in the La Grande that exhibit dextral S-C fabrics.

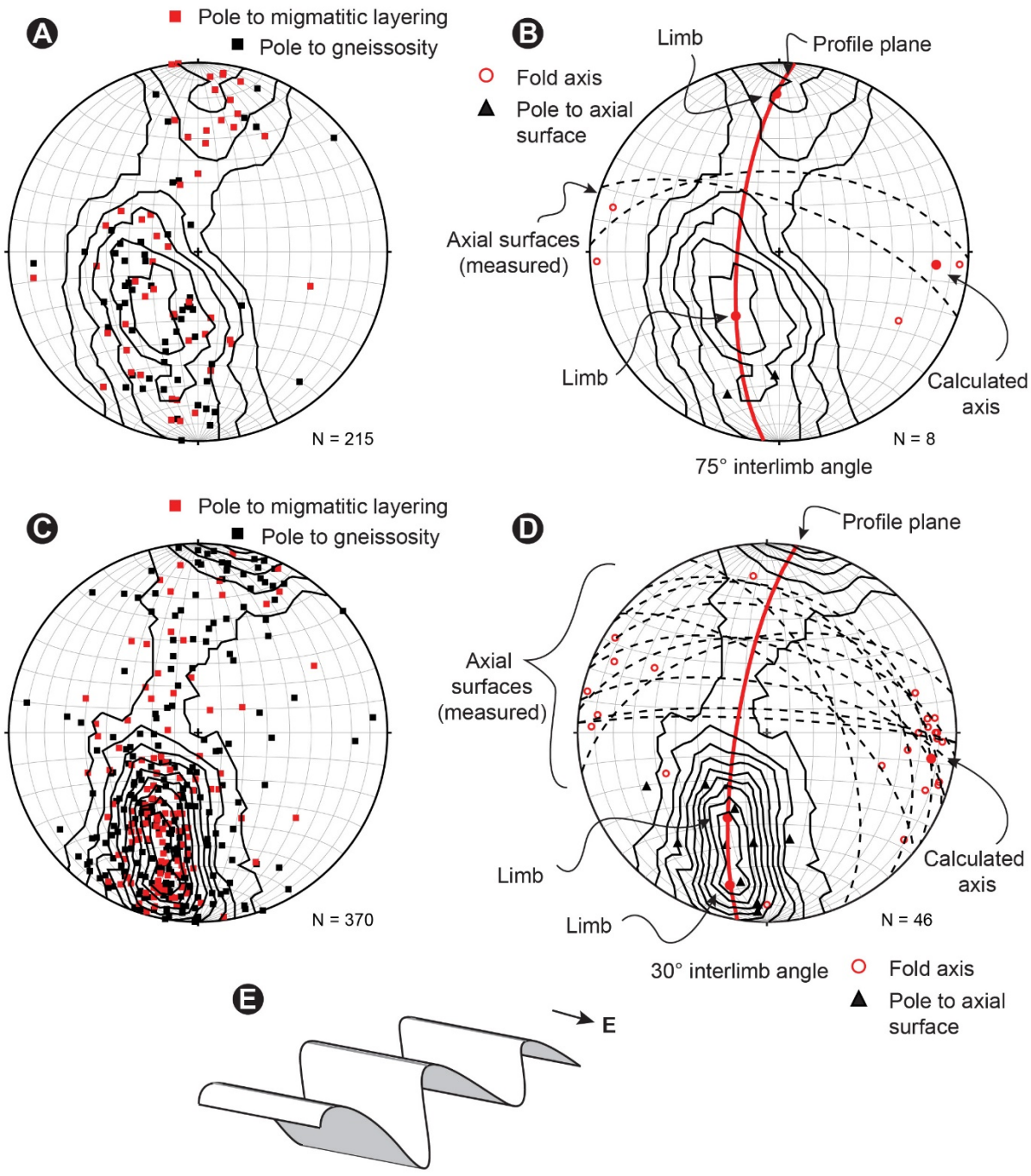

Figure 12: Stereonets for domains I (A and B) and II (C and D) of the Lac Joubert region. A–B) Poles to gneissosity and layering exhibit a spread along a steeply west dipping profile plane, with concentrations in two orientations that are interpreted as general regional limb orientations, despite common local-scale variations. The calculated fold axis in B) is consistent with a small cluster of measured fold axes, and coincident with measured axial surfaces. C–D) Poles to gneissosity and layering are spread throughout a similar profile plane to A-B), except that they are strongly clustered in the southern stereonet hemisphere. Two overlapping clusters represent individual north-dipping limbs, consistent with observed outcrop-scale overturned tight folds. Measured fold axes cluster around the calculated fold axis, plunging shallowly east, and axial plane measurements vary from steeply to shallowly north dipping. E) Schematic of fold morphology and orientation for domains I and II, with the exception that domain II folds are tighter (30° interlimb angle), overturned, and have some variation to their axial surface dip.

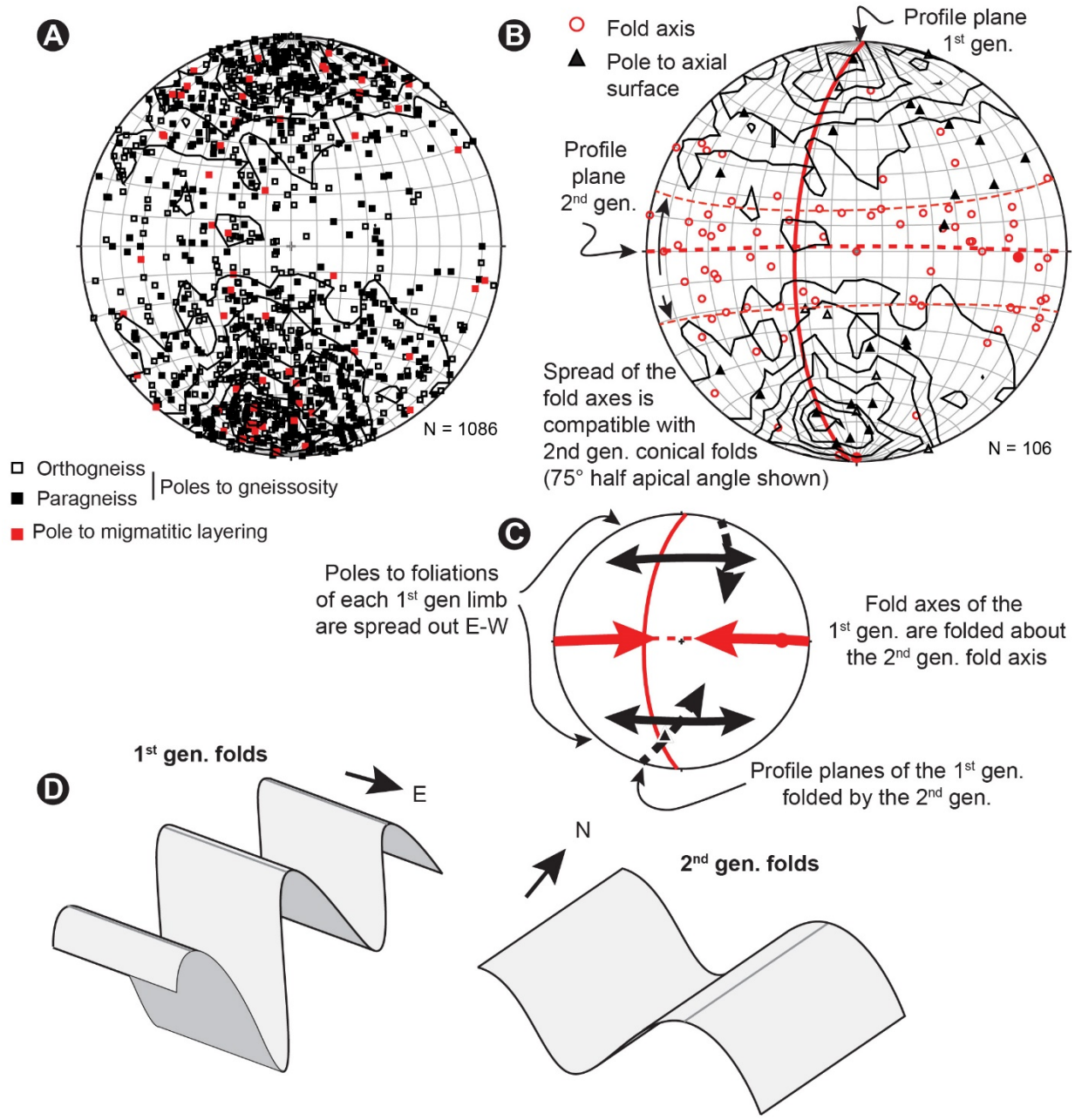

Figure 13: Stereonets for domain III of the Lac Joubert region. A–C) Poles to gneissosity and layering are spread along a similar best-fit profile plane as domains I and II (Figure 12 B and D), except that they show a much wider E-W spread. A minor concentration of measured fold axis measurements cluster around the calculated fold axis, but most are spread evenly along a subvertical E-W oriented great circle This is interpreted to be consistent with a second generation of folding that folded 1st generation fold axes from an original shallowly East plunging orientation. A slight N-S spread to the fold axis measurements along the E-W plane is consistent with a 75° half apical angle conical fold for the 2nd generation, with a subhorizontal N-S fold axis. D) Schematic of fold morphology and orientation for both generations of folds. First generation folds are interpreted to have been similar to folds in the Opinaca (Figure 12 E), and overprinting of 2nd generation open N-S oriented upright folds create the dome and basin pattern seen in the map (Figure 8).

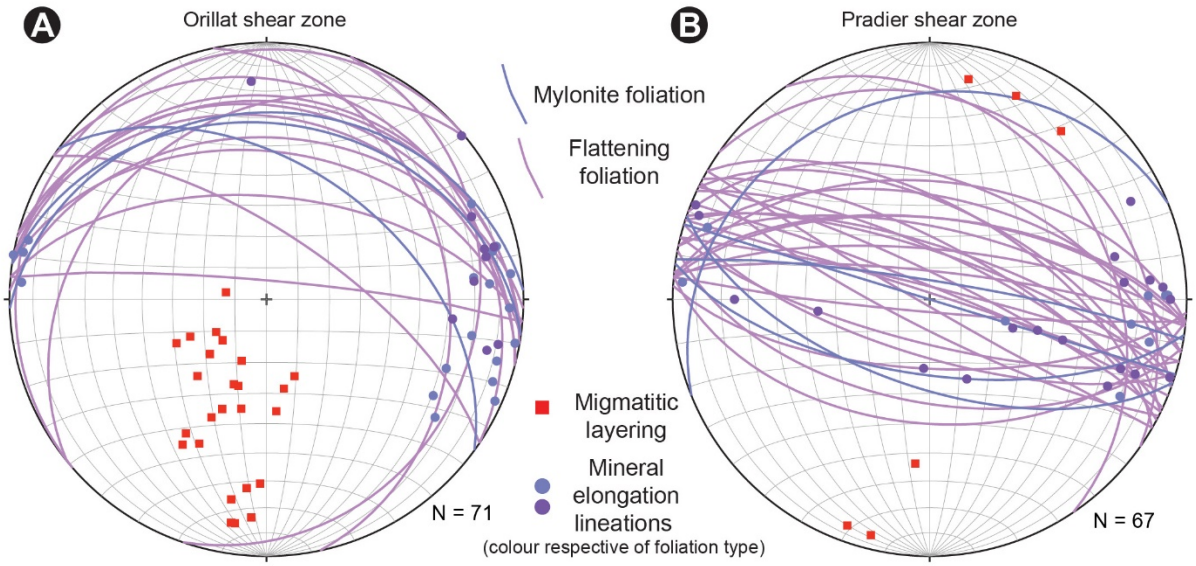

Figure 14: Stereonets for shear zones in domain III of the Lac Joubert region. A) Deformation-related foliations are shallowly dipping north, and their associated mineral elongation lineations plunge shallowly towards the east to east-southeast. B) Deformation-related foliations are moderately to steeply dipping, striking east-southeast, and their associated mineral elongation lineations plunge moderately to shallowly towards the east to east-southeast.

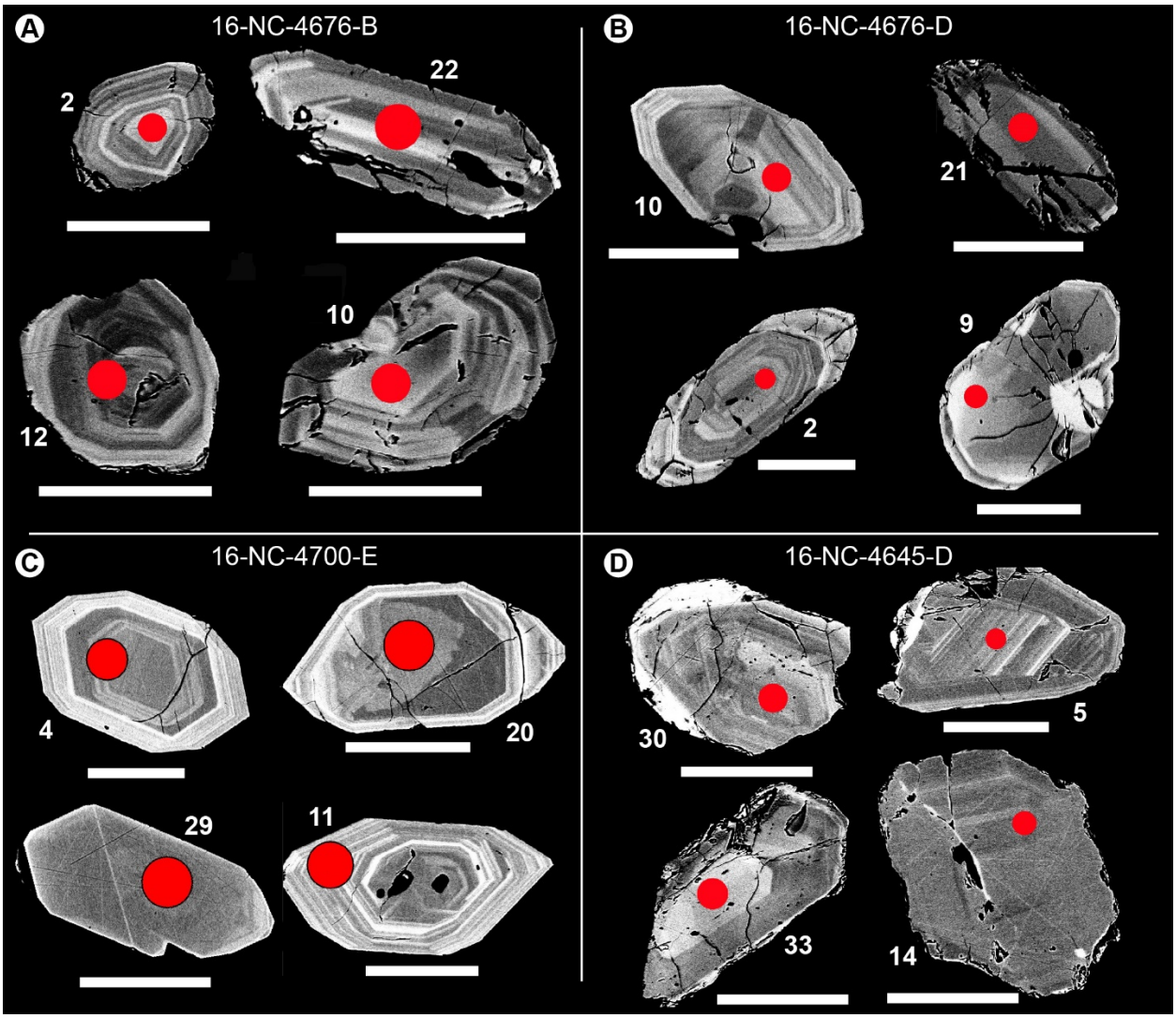

Figure 15: Zircon backscatter electron microscope images for all geochronology samples from the Lac Sakami region. All scale bars represent 100 µm. Spot analyses are indicated in red, and the analysis number is indicated.

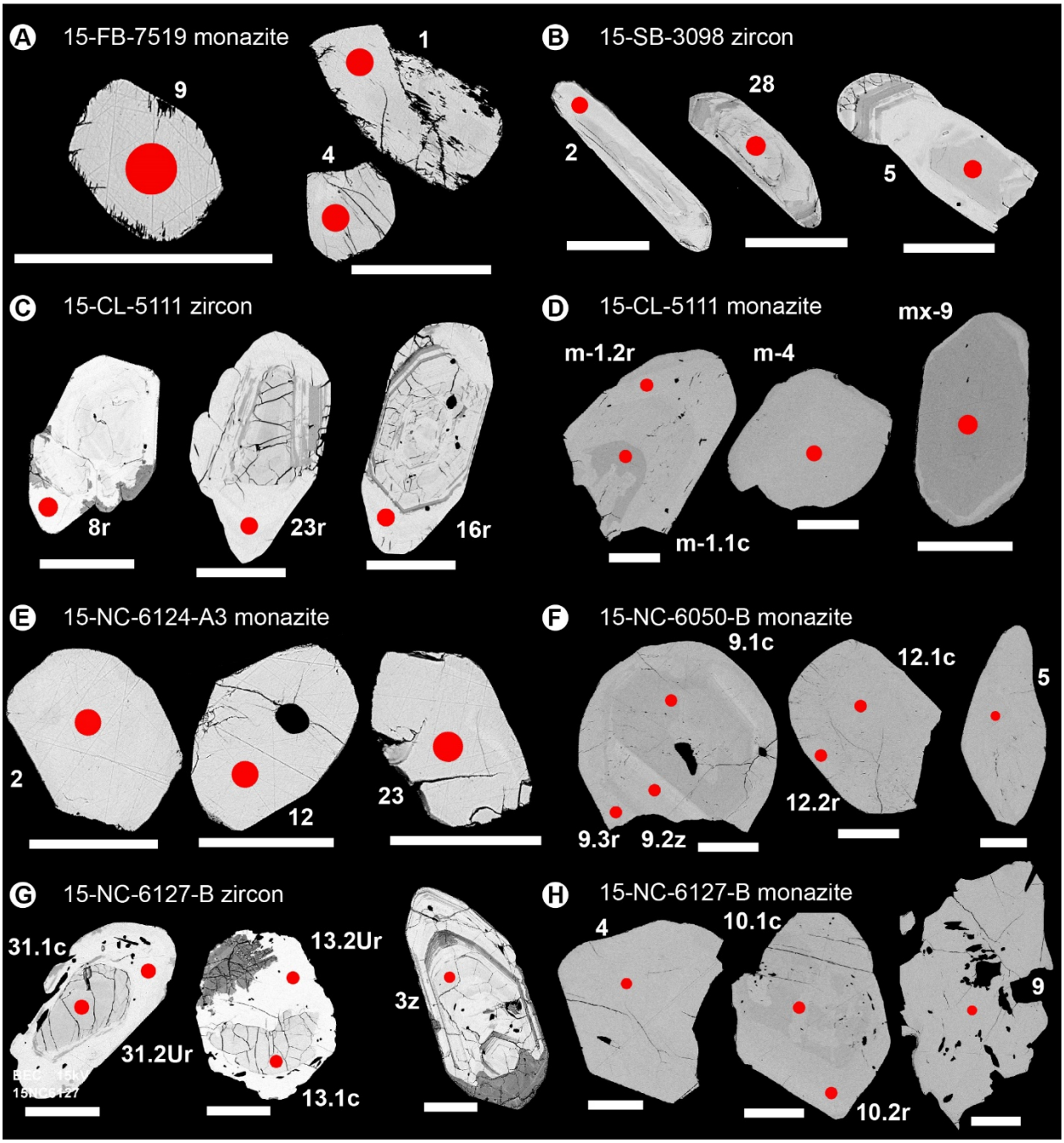

Figure 16: Zircon and monazite backscatter electron microscope images for all geochronology samples from the Lac Joubert region. All scale bars represent 100 µm. Spot analyses are indicated in red, and the analysis number is indicated.

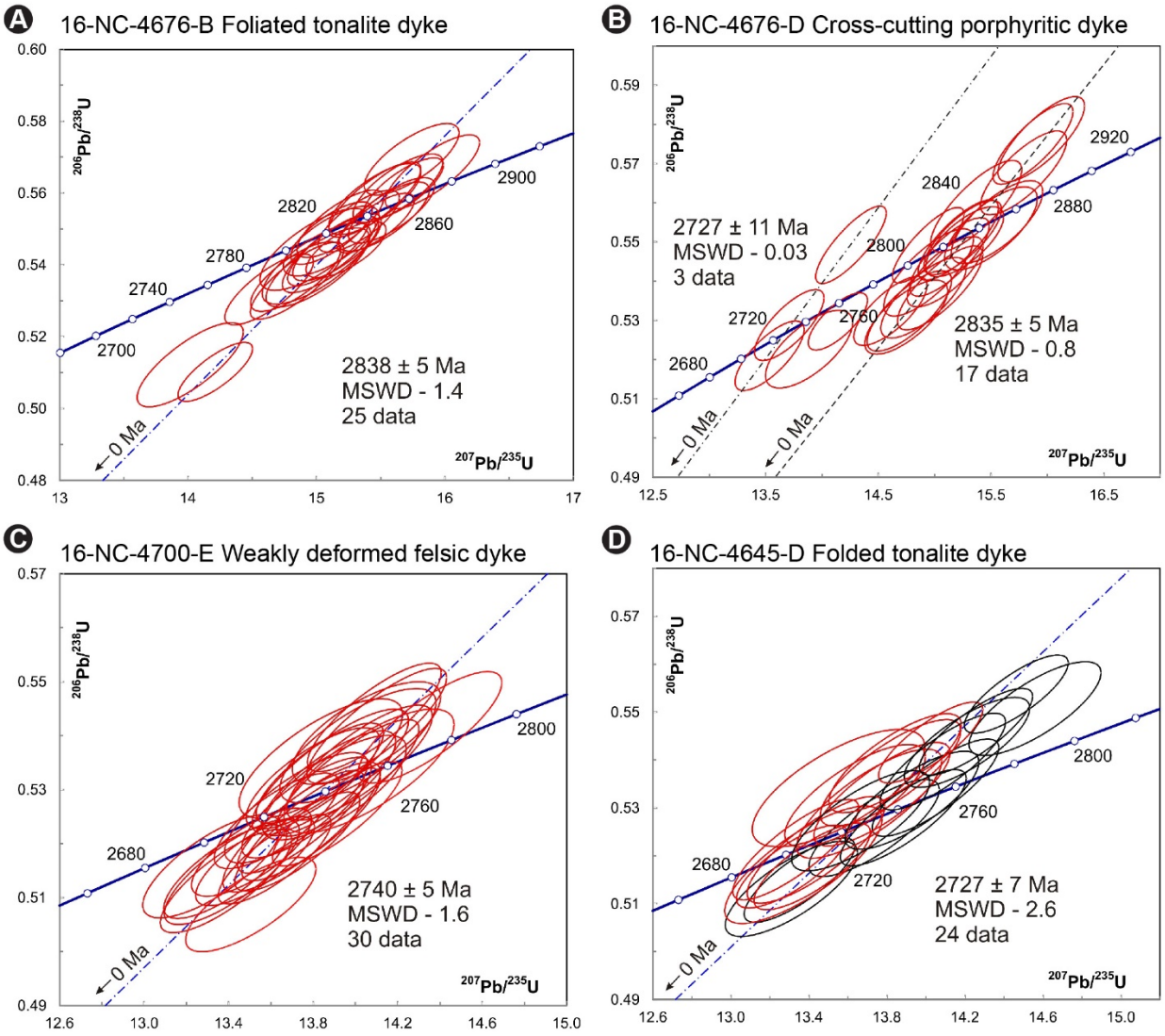

Figure 17: Concordia diagrams for U-Pb zircon LA-ICPMS geochronology from the Lac Sakami region.

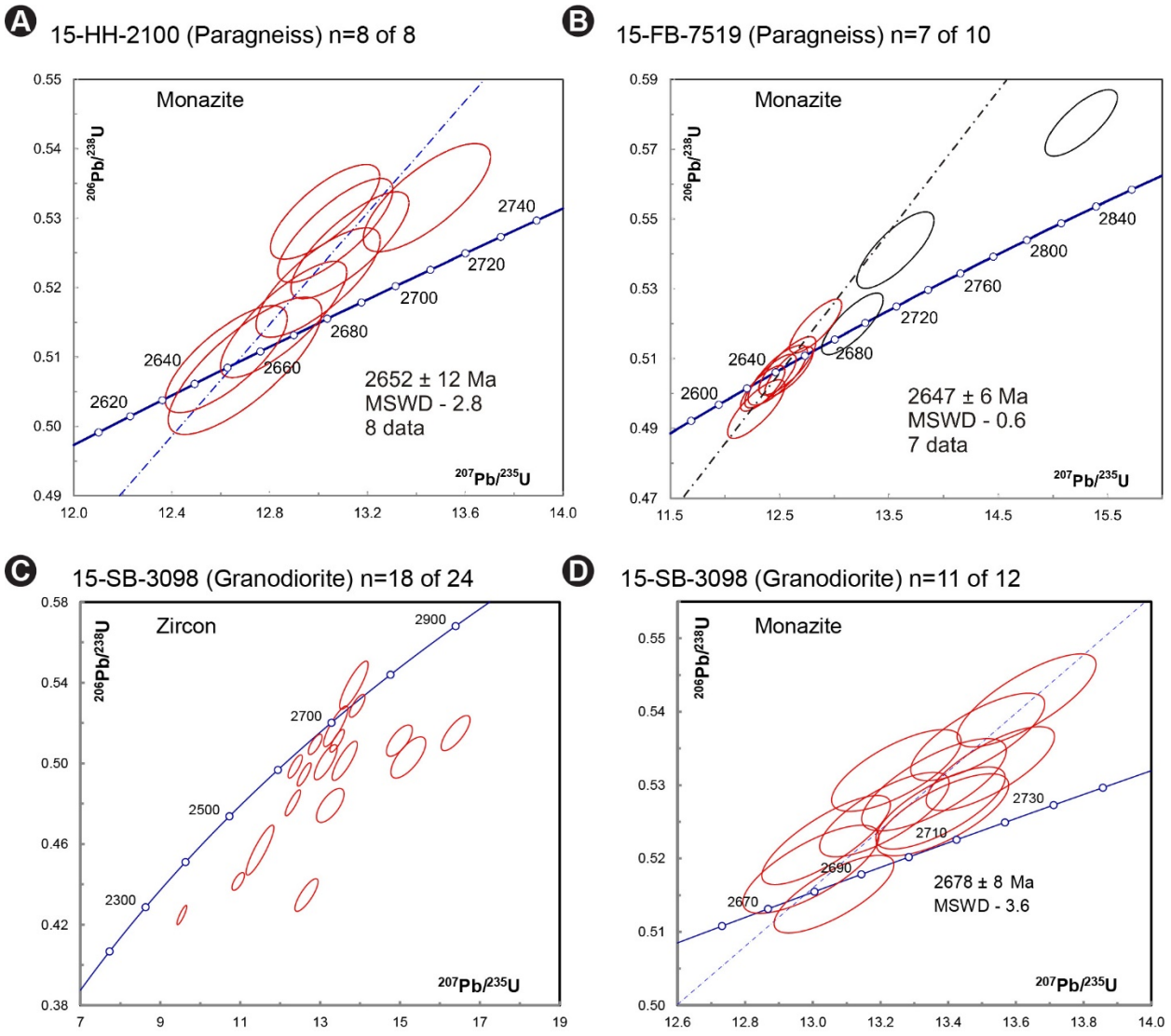

Figure 18: Concordia diagrams for U-Pb zircon and monazite LA-ICPMS geochronology from the Lac Joubert region, domain I (the Opinaca).

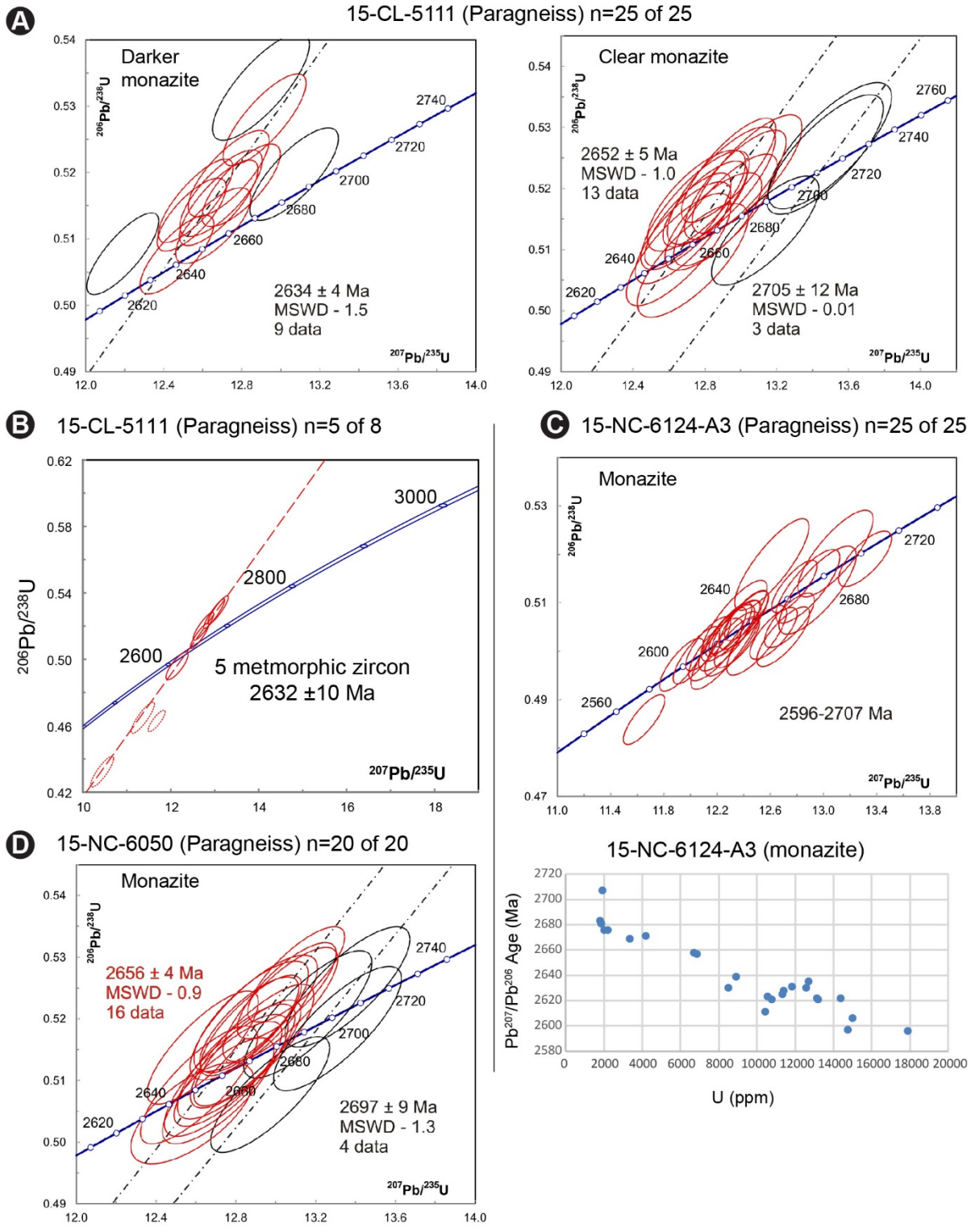

Figure 19: Concordia diagrams for U-Pb zircon and monazite LA-ICPMS geochronology from the Lac Joubert region, domains II and III (the Boisbriand and the La Grande).

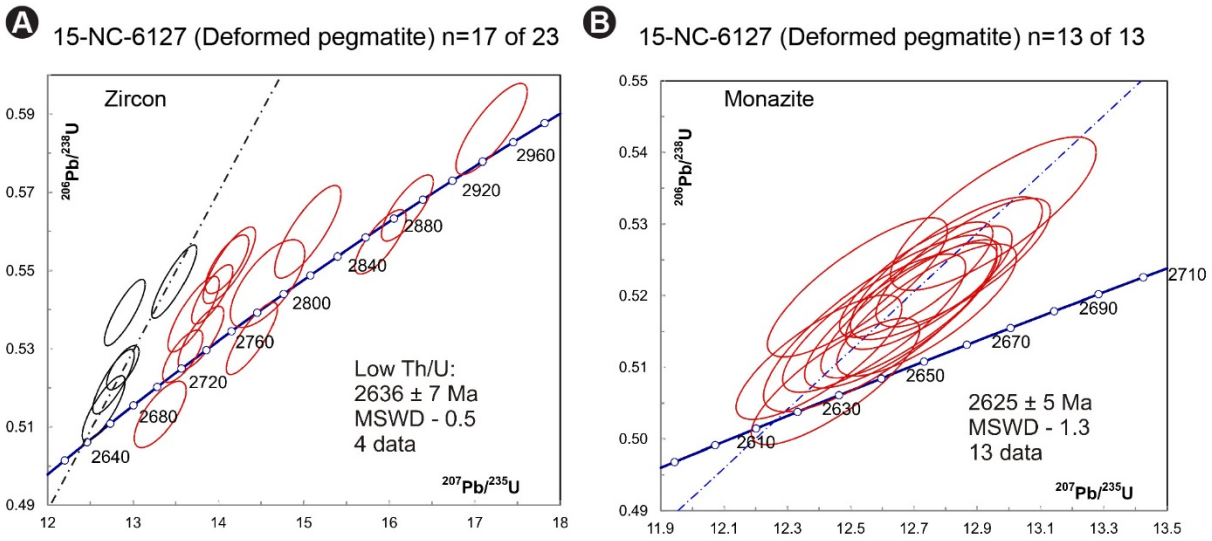

Figure 20: Concordia diagrams for U-Pb zircon and monazite LA-ICPMS geochronology from a pegmatite intrusion in the Lac Joubert region domain III (the La Grande).

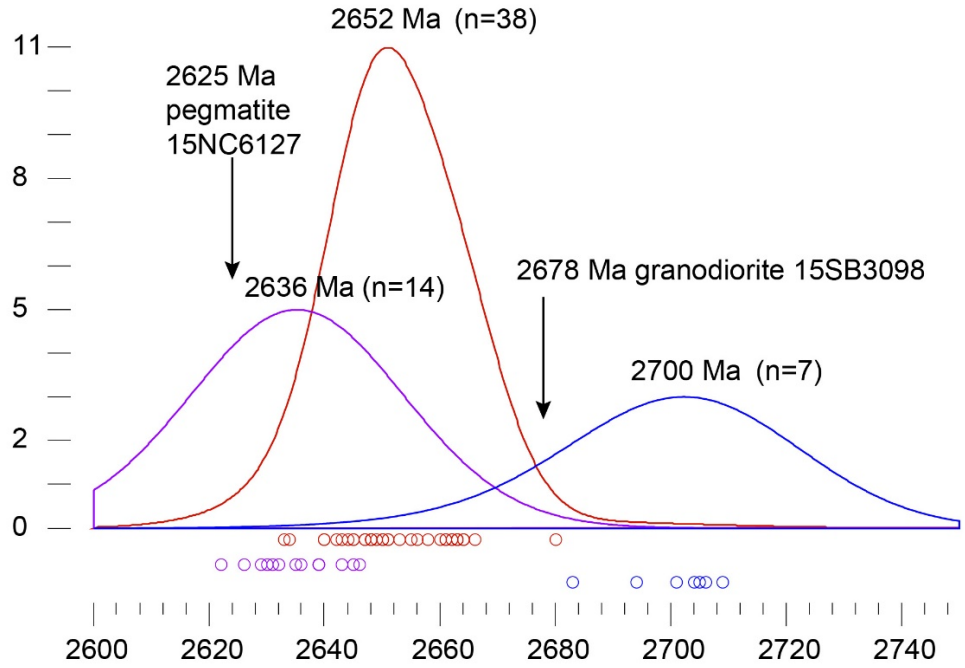

Figure 21: Probability density curves for all monazite and metamorphic single zircon age populations analyzed for each of the three metamorphic events established by Concordia ages. Metamorphic event one at 2700 Ma is established by two Concordia ages that are within error of each other from samples 15-CL-5111 and 15-NC-6050. Metamorphic event two at 2652 Ma is established by four Concordia ages that are within error of each other from samples 15-CL-5111, 15-NC-6050, 15-HH-2100, and 15-FB-7519. Metamorphic event three at 2636 Ma is established by two Concordia ages that are within error of each other from sample 15-CL-5111 (zircon and monazite). These indicate that three metamorphic events generated monazite, and in some cases zircon, at 2700, 2652, and 2636 Ma. Monazite from the 2700 Ma event may be inherited or detrital.

Table 1: LA-ICPMS U-Pb zircon geochronology data for the Lac Sakami region.

Spot	U (ppm)	Pb^{206} (ppm)	Th / U	$^{207}Pb/^{235}U$	1 Sig	$^{206}Pb/^{238}U$	1 Sig	Err. Correl.	$^{207}Pb/^{206}Pb$ Age (Ma)	1 Sig	$^{207}Pb/^{235}U$ Age (Ma)	1 Sig	$^{206}Pb/^{238}U$ Age (Ma)	1 Sig	Disc. (%)
16-NC-4676B	**Foliated tonalite dyke, mount M161229A**														
16NC4676B-4c	253	130	0.54	14.017	0.169	0.5122	0.0048	0.7761	2814	12	2751	11	2666	20	6
16NC4676B-2c	326	174	0.52	14.632	0.141	0.5331	0.0040	0.7836	2818	10	2792	9	2755	17	3
16NC4676B-3	88	48	0.34	14.987	0.174	0.5443	0.0046	0.7336	2824	13	2814	11	2801	19	1
16NC4676B-11c	140	77	0.76	15.186	0.138	0.5514	0.0038	0.7645	2824	10	2827	9	2831	16	0
16NC4676B-12c	131	72	0.81	15.117	0.129	0.5488	0.0035	0.7547	2824	9	2823	8	2820	15	0
16NC4676B-1z	233	125	0.35	14.838	0.143	0.5367	0.0040	0.7626	2830	10	2805	9	2770	17	3
16NC4676B-15	172	98	0.64	15.742	0.151	0.5694	0.0041	0.7435	2830	10	2861	9	2905	17	-3
16NC4676B-13	64	35	0.59	15.115	0.152	0.5466	0.0040	0.7204	2831	11	2823	10	2811	17	1
16NC4676B-17c	234	130	0.66	15.455	0.147	0.5583	0.0040	0.7611	2832	10	2844	9	2860	17	-1
16NC4676B-16	237	132	0.57	15.454	0.147	0.5582	0.0043	0.8066	2833	9	2844	9	2859	18	-1
16NC4676B-9c	171	92	0.64	14.849	0.149	0.5356	0.0044	0.8135	2835	10	2806	10	2765	18	3
16NC4676B-5	192	104	0.76	15.000	0.172	0.5404	0.0046	0.7450	2837	13	2815	11	2785	19	2
16NC4676B-27	671	370	0.37	15.330	0.129	0.5521	0.0035	0.7562	2837	9	2836	8	2834	15	0
16NC4676B-10c	304	165	0.91	15.119	0.140	0.5439	0.0040	0.7933	2839	9	2823	9	2800	17	2
16NC4676B-8c	405	221	0.50	15.150	0.137	0.5445	0.0037	0.7511	2841	10	2825	9	2802	15	2
16NC4676B-18z	149	80	0.57	15.009	0.164	0.5393	0.0045	0.7621	2841	12	2816	10	2780	19	3
16NC4676B-19z	372	202	0.54	15.119	0.158	0.5433	0.0045	0.7968	2841	10	2823	10	2797	19	2
16NC4676B-20c	167	94	0.35	15.635	0.143	0.5613	0.0039	0.7581	2842	10	2855	9	2872	16	-1
16NC4676B-22z	197	100	0.53	14.212	0.119	0.5102	0.0033	0.7859	2843	8	2764	8	2657	14	8
16NC4676B-21z	160	90	0.64	15.679	0.127	0.5612	0.0035	0.7675	2847	8	2857	8	2872	14	-1
16NC4676B-28	172	93	0.43	15.231	0.127	0.5442	0.0032	0.7059	2850	10	2830	8	2801	13	2
16NC4676B-24	155	86	0.39	15.461	0.123	0.5516	0.0034	0.7686	2853	8	2844	8	2832	14	1
16NC4676B-29c	204	113	0.33	15.527	0.144	0.5534	0.0039	0.7663	2854	10	2848	9	2839	16	1
16NC4676B-26	131	73	0.26	15.585	0.138	0.5552	0.0037	0.7574	2855	9	2852	8	2847	15	0
16NC4676B-23	74	42	0.38	15.903	0.150	0.5659	0.0042	0.7900	2857	9	2871	9	2891	17	-1

NOTES:

z - oscillatory zoning; p - patchy zonation; u - homogeneous; c - core; r - thin rim; rnd - rounded; k - cracked

Relation between ages and concordia coordinates: Y = 206Pb/238U = EXP(L238*(206-238Age)) - 1;

X = 207Pb/235U = EXP(L235*(207-235Age)) - 1

207Pb/206Pb = 137.88*X/Y; U decay constants (L238 & L235) from Jaffey et al. (1971).

L238 - 1.55125 X 10^{-4} /Ma; L235 - 9.8485 X 10^{-4} /Ma

Table 1: LA-ICPMS U-Pb zircon geochronology data for the Lac Sakami region.

Spot	U (ppm)	Pb^{206} (ppm)	Th / U	$^{207}Pb/^{235}U$	1 Sig	$^{206}Pb/^{238}U$	1 Sig	Err. Correl.	$^{207}Pb/^{206}Pb$ Age (Ma)	1 Sig	$^{207}Pb/^{235}U$ Age (Ma)	1 Sig	$^{206}Pb/^{238}U$ Age (Ma)	1 Sig	Disc. (%)
16-NC-4676D	**Porphyritic felsic dyke crosscutting regional foliation, mount M161229A**														
NC4676D-10c	183	97	0.39	13.711	0.126	0.5288	0.0037	0.7634	2725	10	2730	9	2736	16	-1
NC4676D-30z	202	111	0.37	14.258	0.127	0.5493	0.0040	0.8218	2727	8	2767	8	2822	17	-4
NC4676D-28	111	58	0.30	13.536	0.125	0.5210	0.0036	0.7538	2729	10	2718	9	2703	15	1
NC4676D-21	110	57	0.48	13.886	0.158	0.5226	0.0040	0.6815	2765	14	2742	11	2710	17	2
NC4676D-32c	243	129	0.40	14.142	0.107	0.5297	0.0030	0.7415	2773	8	2759	7	2740	13	1
NC4676D-31c	173	95	0.54	14.943	0.130	0.5492	0.0039	0.8248	2804	8	2812	8	2822	16	-1
NC4676D-25	130	69	0.38	14.608	0.133	0.5324	0.0036	0.7429	2818	10	2790	9	2752	15	3
NC4676D-8c	119	67	0.58	15.368	0.165	0.5591	0.0048	0.7969	2821	11	2838	10	2863	20	-2
NC4676D-1c	123	66	0.45	14.947	0.162	0.5422	0.0045	0.7718	2826	11	2812	10	2793	19	1
NC4676D-9z	233	134	0.53	15.872	0.145	0.5750	0.0042	0.8020	2828	9	2869	9	2928	17	-4
NC4676D-3z	157	86	0.41	15.210	0.146	0.5505	0.0042	0.7942	2829	9	2828	9	2827	17	0
NC4676D-5	218	120	0.38	15.249	0.140	0.5511	0.0039	0.7630	2832	10	2831	9	2830	16	0
NC4676D-19	169	97	0.48	15.946	0.157	0.5762	0.0044	0.7823	2832	10	2874	9	2933	18	-4
NC4676D-29c	147	81	0.31	15.132	0.144	0.5462	0.0041	0.7877	2834	10	2824	9	2809	17	1
NC4676D-14z	136	75	0.70	15.266	0.141	0.5501	0.0036	0.7156	2837	11	2832	9	2826	15	0
NC4676D-24	123	65	0.32	14.776	0.153	0.5324	0.0042	0.7600	2837	11	2801	10	2752	18	4
NC4676D-16z	137	73	0.55	14.748	0.150	0.5308	0.0039	0.7154	2838	12	2799	10	2745	16	4
NC4676D-12c	104	59	0.64	15.789	0.156	0.5676	0.0044	0.7787	2840	10	2864	9	2898	18	-3
NC4676D-17	193	103	0.72	14.902	0.155	0.5358	0.0042	0.7548	2840	11	2809	10	2766	18	3
NC4676D-20	235	127	0.40	15.093	0.138	0.5424	0.0037	0.7407	2841	10	2821	9	2794	15	2
NC4676D-2c	171	92	0.28	15.049	0.154	0.5383	0.0044	0.7911	2849	10	2818	10	2776	18	3
NC4676D-15z	81	45	0.36	15.499	0.168	0.5535	0.0043	0.7204	2851	12	2846	10	2840	18	1
NC4676D-13z	88	49	0.52	15.553	0.166	0.5551	0.0043	0.7304	2852	12	2850	10	2846	18	0

Table 1: LA-ICPMS U-Pb zircon geochronology data for the Lac Sakami region.

Spot	U (ppm)	Pb^{206} (ppm)	Th / U	$^{207}Pb/^{235}U$	1 Sig	$^{206}Pb/^{238}U$	1 Sig	Err. Correl.	$^{207}Pb/^{206}Pb$ Age (Ma)	1 Sig	$^{207}Pb/^{235}U$ Age (Ma)	1 Sig	$^{206}Pb/^{238}U$ Age (Ma)	1 Sig	Disc. (%)
16-NC-4700E	**Felsic dyke crosscutting regional foliation, mount M170222**														
16NC4700-4z	82	42	0.36	13.320	0.133	0.5158	0.0039	0.7543	2719	11	2703	9	2681	17	2
16NC4700-29u	42	22	0.63	13.837	0.158	0.5357	0.0045	0.7389	2719	13	2739	11	2766	19	-2
16NC4700-22z	69	37	0.34	13.798	0.129	0.5321	0.0038	0.7692	2725	10	2736	9	2750	16	-1
16NC4700-23zck	99	54	0.41	14.090	0.129	0.5434	0.0041	0.8234	2725	9	2756	9	2798	17	-3
16NC4700-12p	136	72	0.17	13.832	0.123	0.5330	0.0038	0.8013	2727	9	2738	8	2754	16	-1
16NC4700-7c	101	53	0.50	13.627	0.121	0.5242	0.0036	0.7778	2730	9	2724	8	2717	15	1
16NC4700-8z	55	30	0.30	14.052	0.143	0.5405	0.0039	0.7049	2730	12	2753	10	2785	16	-3
16NC4700-30z	124	64	0.51	13.384	0.119	0.5148	0.0035	0.7768	2730	9	2707	8	2677	15	2
16NC4700-32z	135	73	0.43	14.101	0.135	0.5418	0.0044	0.8410	2731	9	2757	9	2791	18	-3
16NC4700-6c	78	42	0.39	13.881	0.151	0.5333	0.0047	0.8171	2732	10	2742	10	2755	20	-1
16NC4700-24uc	35	19	0.37	14.012	0.151	0.5381	0.0043	0.7465	2732	12	2751	10	2776	18	-2
16NC4700-11z	128	67	0.33	13.508	0.116	0.5184	0.0033	0.7482	2733	9	2716	8	2692	14	2
16NC4700-27u	66	35	0.46	13.719	0.138	0.5266	0.0042	0.7892	2733	10	2731	10	2727	18	0
16NC4700-1z	86	44	0.34	13.415	0.130	0.5147	0.0040	0.7937	2734	10	2709	9	2677	17	3
16NC4700-5rnd	108	55	0.70	13.388	0.127	0.5131	0.0039	0.8041	2736	9	2707	9	2670	17	3
16NC4700-20pc	88	47	0.48	13.873	0.130	0.5312	0.0040	0.7962	2737	9	2741	9	2746	17	0
16NC4700-25pc	83	44	0.33	13.769	0.125	0.5266	0.0038	0.7950	2739	9	2734	9	2727	16	1
16NC4700-31z	134	69	0.50	13.525	0.115	0.5167	0.0034	0.7684	2741	9	2717	8	2685	14	2
16NC4700-10uc	39	20	0.39	13.901	0.139	0.5304	0.0040	0.7447	2743	11	2743	9	2743	17	0
16NC4700-14zc	92	49	0.43	14.019	0.141	0.5350	0.0043	0.8095	2743	10	2751	10	2762	18	-1
16NC4700-15cku	252	132	0.60	13.742	0.122	0.5240	0.0039	0.8319	2744	8	2732	8	2716	16	1
16NC4700-21z	108	57	0.36	13.963	0.138	0.5322	0.0044	0.8392	2745	9	2747	9	2751	19	0
16NC4700-17zc	108	56	0.39	13.745	0.152	0.5230	0.0049	0.8483	2747	10	2732	10	2712	21	2
16NC4700-2uc	293	151	0.60	13.618	0.109	0.5171	0.0034	0.8153	2751	8	2723	8	2687	14	3
16NC4700-19uc	162	85	0.50	13.790	0.134	0.5236	0.0043	0.8393	2751	9	2735	9	2714	18	2
16NC4700-9uc	137	72	0.49	13.725	0.121	0.5204	0.0037	0.8157	2753	8	2731	8	2701	16	2
16NC4700-26u	34	18	0.34	14.064	0.165	0.5334	0.0047	0.7498	2753	13	2754	11	2756	20	0
16NC4700-13uc	146	77	0.49	13.914	0.125	0.5255	0.0039	0.8326	2760	8	2744	9	2722	17	2
16NC4700-28uc	82	44	0.53	14.352	0.139	0.5415	0.0042	0.8053	2761	9	2773	9	2790	18	-1
16NC4700-16pc	131	66	0.63	13.505	0.126	0.5087	0.0036	0.7526	2764	10	2716	9	2651	15	5

Table 1: LA-ICPMS U-Pb zircon geochronology data for the Lac Sakami region.

Spot	U (ppm)	Pb^{206} (ppm)	Th / U	$^{207}Pb/^{235}U$	1 Sig	$^{206}Pb/^{238}U$	1 Sig	Err. Correl.	$^{207}Pb/^{206}Pb$ Age (Ma)	1 Sig	$^{207}Pb/^{235}U$ Age (Ma)	1 Sig	$^{206}Pb/^{238}U$ Age (Ma)	1 Sig	Disc. (%)
16-NC-4645D	**Folded tonalite dyke crosscutting gabbro mylonites, mount M161229A**														
14NC4645D-20	38	20	0.28	13.582	0.197	0.5341	0.0050	0.6459	2693	18	2721	14	2759	21	-3
14NC4645D-15z	104	54	0.71	13.291	0.150	0.5213	0.0043	0.7273	2698	13	2701	11	2705	18	0
14NC4645D-36c	50	27	0.54	13.774	0.146	0.5393	0.0042	0.7385	2700	12	2734	10	2781	18	-4
14NC4645D-17	60	32	0.53	13.630	0.161	0.5326	0.0044	0.6932	2704	14	2724	11	2752	18	-2
14NC4645D-33c	119	65	0.86	13.960	0.116	0.5436	0.0034	0.7642	2709	9	2747	8	2799	14	-4
14NC4645D-13c	137	71	0.44	13.297	0.131	0.5177	0.0035	0.6935	2710	12	2701	9	2690	15	1
14NC4645D-14	75	39	0.62	13.398	0.161	0.5212	0.0046	0.7268	2711	14	2708	11	2704	19	0
14NC4645D-16	51	27	0.52	13.348	0.176	0.5181	0.0050	0.7309	2715	15	2705	12	2691	21	1
14NC4645D-23	92	49	0.98	13.850	0.164	0.5373	0.0045	0.7155	2716	14	2739	11	2772	19	-3
14NC4645D-19	72	38	0.17	13.720	0.171	0.5309	0.0047	0.7042	2720	15	2731	12	2745	20	-1
14NC4645D-12c	85	44	0.59	13.421	0.134	0.5178	0.0037	0.7158	2725	11	2710	9	2690	16	2
14NC4645D-28	69	36	0.69	13.678	0.169	0.5273	0.0043	0.6560	2726	15	2728	12	2730	18	0
14NC4645D-5c	97	52	0.16	13.836	0.156	0.5328	0.0044	0.7348	2728	13	2739	11	2753	19	-1
14NC4645D-32c	50	27	0.71	14.035	0.141	0.5397	0.0041	0.7630	2730	11	2752	9	2782	17	-2
14NC4645D-38c	119	65	1.01	14.195	0.125	0.5459	0.0037	0.7723	2730	9	2763	8	2808	15	-4
14NC4645D-39c	123	68	0.75	14.405	0.119	0.5537	0.0033	0.7279	2731	9	2777	8	2841	14	-5
14NC4645D-10c	115	59	0.53	13.403	0.132	0.5149	0.0036	0.7111	2732	11	2708	9	2678	15	2
14NC4645D-9c	48	25	0.04	13.365	0.150	0.5131	0.0041	0.7063	2733	13	2706	11	2670	17	3
14NC4645D-31c	59	32	0.86	14.180	0.143	0.5437	0.0038	0.7015	2735	12	2762	10	2799	16	-3
14NC4645D-11c	88	46	0.46	13.760	0.151	0.5258	0.0041	0.7187	2740	13	2733	10	2724	17	1
14NC4645D-25	104	55	0.77	13.962	0.160	0.5316	0.0042	0.6875	2746	14	2747	11	2748	18	0
14NC4645D-27c	106	56	0.62	13.918	0.160	0.5279	0.0041	0.6756	2753	14	2744	11	2733	17	1
14NC4645D-1c	110	59	0.85	14.116	0.153	0.5342	0.0041	0.7145	2756	12	2758	10	2759	17	0
14NC4645D-30c	69	38	0.71	14.550	0.156	0.5507	0.0040	0.6768	2756	13	2786	10	2828	17	-3

Table 2: LA-ICPMS U-Pb zircon and monazite geochronology data for the Lac Joubert region.

Spot	U (ppm)	Pb^{206} (ppm)	Th/U	$^{207}Pb/^{235}U$	1 Sig	$^{206}Pb/^{238}U$	1 Sig	Err. Correl.	$^{207}Pb/^{206}Pb$ Age (Ma)	1 Sig	$^{207}Pb/^{235}U$ Age (Ma)	1 Sig	$^{206}Pb/^{238}U$ Age (Ma)	1 Sig	Disc. (%)
15-HH-2100	**Monazite**														
15-HH-2100-mz-1	8888	4581	--	12.857	0.10548	0.5154	0.0034	0.8116	2661	8	2669	8	2680	15	-1
15-HH-2100-mz-2	8560	4503	--	13.128	0.09848	0.5261	0.0031	0.7964	2662	8	2689	7	2725	13	-3
15-HH-2100-mz-3	11696	6178	--	13.069	0.09625	0.5282	0.0031	0.7862	2648	8	2685	7	2734	13	-4
15-HH-2100-mz-4	7102	3785	--	13.443	0.10637	0.5329	0.0032	0.7565	2680	9	2711	7	2754	13	-3
15-HH-2100-mz-5	12657	6451	--	12.622	0.10191	0.5097	0.0031	0.7644	2649	9	2652	8	2655	13	0
15-HH-2100-mz-6	13419	7124	--	13.027	0.09118	0.5309	0.0028	0.7510	2634	8	2682	7	2745	12	-5
15-HH-2100-mz-7	9028	4701	--	12.999	0.10369	0.5207	0.0032	0.7744	2663	8	2680	8	2702	14	-2
15-HH-2100-mz-8	2455	1249	--	12.700	0.12839	0.5087	0.0040	0.7862	2663	10	2658	10	2651	17	1
15-FB-7519	**Monazite**														
15-FB-7519-mz-1	2358	1192	--	12.48	0.11065	0.5053	0.0035	0.7822	2645	9	2641	8	2636	15	0
15-FB-7519-mz-2	3408	1968	--	15.26	0.13478	0.5775	0.0039	0.7624	2756	9	2832	8	2939	16	-8
15-FB-7519-mz-3	5002	2479	--	12.29	0.10724	0.4956	0.0034	0.7921	2651	9	2627	8	2595	15	3
15-FB-7519-mz-4	5213	2710	--	13.17	0.11491	0.5199	0.0036	0.7942	2686	9	2692	8	2699	15	-1
15-FB-7519-mz-5	6003	3049	--	12.57	0.10619	0.5079	0.0034	0.7992	2648	8	2648	8	2648	15	0
15-FB-7519-mz-6	5033	2614	--	12.83	0.09733	0.5193	0.0031	0.7978	2645	8	2667	7	2696	13	-2
15-FB-7519-mz-7	4072	2062	--	12.587	0.09052	0.5063	0.0029	0.7976	2656	7	2649	7	2641	12	1
15-FB-7519-mz-8	5861	2951		12.416	0.09581	0.5036	0.0031	0.8037	2642	8	2636	7	2629	13	1
15-FB-7519-mz-9	3662	1837		12.346	0.08348	0.5015	0.0027	0.7835	2640	7	2631	6	2620	11	1
15-FB-7519-mz-10	1542	834		13.559	0.14426	0.5411	0.0045	0.7780	2669	11	2719	10	2788	19	-5

Table 2: LA-ICPMS U-Pb zircon and monazite geochronology data for the Lac Joubert region.

Spot	U (ppm)	Pb^{206} (ppm)	Th/U	$^{207}Pb/^{235}U$	1 Sig	$^{206}Pb/^{238}U$	1 Sig	Err. Correl.	$^{207}Pb/^{206}Pb$ Age (Ma)	1 Sig	$^{207}Pb/^{235}U$ Age (Ma)	1 Sig	$^{206}Pb/^{238}U$ Age (Ma)	1 Sig	Disc. (%)
15-SB-3098	**Deformed granodiorite**														
Zircon															
15-SB-3098-77*	1857	789	0.06	9.540	0.05047	0.4248	0.0020	0.8776	2486	4	2391	5	2282	9	10
15-SB-3098-5*	1173	518	0.05	10.950	0.06391	0.4415	0.0018	0.6971	2652	7	2519	5	2357	8	13
15-SB-3098-11*	747	372	0.05	12.376	0.07293	0.4985	0.0024	0.8003	2653	6	2633	6	2607	10	2
15-SB-3098-21	548	250	0.04	11.495	0.14253	0.4570	0.0051	0.8941	2675	9	2564	12	2426	22	11
15-SB-3098-12	588	300	0.05	12.876	0.07051	0.5095	0.0021	0.7400	2683	6	2671	5	2654	9	1
15-SB-3098-38	671	332	0.04	12.603	0.07101	0.4945	0.0024	0.8487	2697	5	2650	5	2590	10	5
15-SB-3098-20*	648	311	0.31	12.320	0.07817	0.4804	0.0026	0.8647	2707	5	2629	6	2529	11	8
15-SB-3098-28	429	231	0.46	13.846	0.14590	0.5388	0.0049	0.8584	2711	9	2739	10	2778	20	-3
15-SB-3098-13zc	363	188	0.49	13.393	0.12462	0.5184	0.0041	0.8560	2719	8	2708	9	2693	18	1
15-SB-3098-5c	247	124	0.27	13.140	0.11748	0.5006	0.0036	0.7959	2745	9	2690	8	2616	15	6
15-SB-3098-15*	641	328	0.02	13.426	0.07365	0.5112	0.0023	0.8213	2746	5	2710	5	2662	10	4
15-SB-3098-2	641	339	0.04	13.929	0.07992	0.5285	0.0023	0.7619	2752	6	2745	5	2735	10	1
15-SB-3098-26	768	385	0.04	13.618	0.12888	0.5013	0.0040	0.8376	2802	8	2723	9	2619	17	8
15-SB-3098-21*	625	300	0.04	13.255	0.14122	0.4792	0.0034	0.6732	2831	13	2698	10	2524	15	13
15-SB-3098-41*	997	433	0.05	12.659	0.11853	0.4347	0.0033	0.8151	2915	9	2655	9	2327	15	24
15-SB-3098-30*	372	190	0.10	14.985	0.13288	0.5113	0.0032	0.6988	2925	10	2814	8	2662	14	11
15-SB-3098-2	750	377	0.29	15.209	0.17844	0.5030	0.0042	0.7078	2976	13	2828	11	2626	18	14
15-SB-3098-69	389	201	0.25	16.393	0.14827	0.5150	0.0036	0.7642	3058	9	2900	9	2678	15	15
15-SB-3098	**Monazite**														
15-SB-3098mz-8m	4135	2200	--	13.247	0.07819	0.5320	0.0023	0.7242	2658	7	2697	6	2750	10	-4
15-SB-3098mz-4m	4749	2481	--	13.039	0.07763	0.5225	0.0025	0.7975	2662	6	2682	6	2710	10	-2
15-SB-3098mz-5	1812	940	--	12.994	0.08219	0.5185	0.0025	0.7480	2669	7	2679	6	2693	10	-1
15-SB-3098mz-6m	3860	2030	--	13.211	0.07823	0.5260	0.0024	0.7547	2673	6	2695	6	2725	10	-2
15-SB-3098mz-13m	2620	1406	--	13.487	0.08097	0.5366	0.0024	0.7556	2674	7	2714	6	2769	10	-4
15-SB-3098mz-14m	5564	3013	--	13.632	0.08390	0.5415	0.0026	0.7768	2676	6	2724	6	2790	11	-5
15-SB-3098mz-9	1454	771	--	13.358	0.08735	0.5301	0.0026	0.7412	2678	7	2705	6	2742	11	-3
15-SB-3098mz-7m	2868	1477	--	13.062	0.07236	0.5152	0.0022	0.7577	2688	6	2684	5	2679	9	0
15-SB-3098mz-11m	1606	846	--	13.377	0.07817	0.5269	0.0023	0.7419	2691	6	2707	6	2728	10	-2
15-SB-3098mz-1	3868	2059	--	13.524	0.07753	0.5323	0.0023	0.7651	2692	6	2717	5	2751	10	-3
15-SB-3098mz-10	1444	759	--	13.383	0.07992	0.5260	0.0023	0.7262	2694	7	2707	6	2724	10	-1

Table 2: LA-ICPMS U-Pb zircon and monazite geochronology data for the Lac Joubert region.

Spot	U (ppm)	Pb^{206} (ppm)	Th/U	$^{207}Pb/^{235}U$	1 Sig	$^{206}Pb/^{238}U$	1 Sig	Err. Correl.	$^{207}Pb/^{206}Pb$ Age (Ma)	1 Sig	$^{207}Pb/^{235}U$ Age (Ma)	1 Sig	$^{206}Pb/^{238}U$ Age (Ma)	1 Sig	Disc. (%)
15-CL-5111	**Clear Monazite**														
15-CL-5111-m-1.1c	3184	1665	--	12.932	0.10724	0.5230	0.0035	0.8012	2647	8	2675	8	2712	15	-3
15-CL-5111-m-1.2r	1760	906	--	12.706	0.09812	0.5149	0.0031	0.7822	2643	8	2658	7	2678	13	-2
15-CL-5111-m-2.1c	3350	1733	--	12.801	0.09571	0.5174	0.0029	0.7416	2648	8	2665	7	2688	12	-2
15-CL-5111-m-2.2r	2090	1083	--	12.754	0.11188	0.5180	0.0034	0.7425	2640	10	2662	8	2691	14	-2
15-CL-5111-m-3.1c	2516	1299	--	12.746	0.12306	0.5164	0.0040	0.7958	2644	10	2661	9	2684	17	-2
15-CL-5111-m-3.2r	1904	976	--	12.679	0.10868	0.5128	0.0034	0.7731	2647	9	2656	8	2668	14	-1
15-CL-5111-m-4	2322	1209	--	12.892	0.12299	0.5205	0.0039	0.7906	2650	10	2672	9	2701	17	-2
15-CL-5111-m-8r	1873	961	--	13.137	0.12185	0.5131	0.0036	0.7665	2704	10	2690	9	2670	16	2
15-CL-5111-m-6.1c	2506	1274	--	12.732	0.12594	0.5082	0.0038	0.7562	2668	11	2660	9	2649	16	1
15-CL-5111-m-6.2r	2591	1321	--	12.655	0.11895	0.5100	0.0038	0.7845	2653	10	2654	9	2657	16	0
15-CL-5111-m-7.1c	2189	1126		12.847	0.11002	0.5146	0.0033	0.7398	2663	10	2669	8	2676	14	-1
15-CL-5111-m-7.2r	2840	1497		13.496	0.14028	0.5270	0.0042	0.7707	2705	11	2715	10	2729	18	-1
15-CL-5111-m-9	2975	1554		13.036	0.12496	0.5223	0.0040	0.7917	2662	10	2682	9	2709	17	-2
15-CL-5111-m-10	5794	3016		12.969	0.11554	0.5206	0.0037	0.7874	2659	9	2677	8	2702	15	-2
15-CL-5111-m-11.1c	7239	3739		12.915	0.11750	0.5165	0.0037	0.7957	2665	9	2673	9	2684	16	-1
15-CL-5111-m-11.2r	2801	1472		13.469	0.13276	0.5256	0.0040	0.7720	2706	10	2713	9	2723	17	-1
	Dark Monazite														
15-CL-5111-mx-1	4449	2293	--	12.682	0.08234	0.5154	0.0026	0.7856	2639	7	2656	6	2680	11	-2
15-CL-5111-mx-2	3270	1694	--	12.797	0.08203	0.5181	0.0025	0.7655	2645	7	2665	6	2691	11	-2
15-CL-5111-mx-3.1c	3405	1770	--	12.733	0.08487	0.5198	0.0027	0.7663	2631	7	2660	6	2698	11	-3
15-CL-5111-mx-4	3943	2038	--	12.694	0.08625	0.5169	0.0027	0.7586	2635	7	2657	6	2686	11	-2
15-CL-5111-mx-5	3785	1921	--	12.468	0.07704	0.5076	0.0024	0.7736	2636	6	2640	6	2647	10	-1
15-CL-5111-mx-8	5013	2646	--	12.917	0.08669	0.5280	0.0028	0.7979	2629	7	2674	6	2733	12	-5
15-CL-5111-mx-7.1c	3736	1913	--	12.654	0.07875	0.5120	0.0023	0.7311	2646	7	2654	6	2665	10	-1
15-CL-5111-mx-9	5491	2820	--	12.543	0.07218	0.5136	0.0022	0.7592	2626	6	2646	5	2672	10	-2
15-CL-5111-mx-10	4471	2306	--	12.564	0.07832	0.5157	0.0026	0.7996	2622	6	2648	6	2681	11	-3
15-CL-5111	**Metamorphic zircon**														
15-CL-5111-23r	2695	1337	0.03	12.139	0.10255	0.4960	0.0034	0.8106	2630	8	2615	8	2597	15	2
15-CL-5111-16r	1294	673	0.01	12.741	0.09558	0.5199	0.0034	0.8816	2632	6	2661	7	2699	15	-3
15-CL-5111-6r	617	317	0.02	12.652	0.08616	0.5142	0.0031	0.8949	2639	5	2654	6	2674	13	-2
15-CL-5111-8r	630	332	0.02	12.986	0.09786	0.5275	0.0037	0.9214	2639	5	2679	7	2731	15	-4
15-CL-5111-13.2c	1049	556	0.01	13.075	0.09475	0.5298	0.0034	0.8974	2643	5	2685	7	2741	15	-5

Table 2: LA-ICPMS U-Pb zircon and monazite geochronology data for the Lac Joubert region.

Spot	U (ppm)	Pb^{206} (ppm)	Th/U	$^{207}Pb/^{235}U$	1 Sig	$^{206}Pb/^{238}U$	1 Sig	Err. Correl.	$^{207}Pb/^{206}Pb$ Age (Ma)	1 Sig	$^{207}Pb/^{235}U$ Age (Ma)	1 Sig	$^{206}Pb/^{238}U$ Age (Ma)	1 Sig	Disc. (%)
15-NC-6124	**Monazite**														
15-NC-6124-A3-mz-8	17873	8684	--	11.653	0.06346	0.4859	0.0021	0.7933	2596	6	2577	5	2553	9	2
15-NC-6124-A3-mz-5	14755	7336	--	11.935	0.06787	0.4972	0.0022	0.7895	2597	6	2599	5	2602	10	0
15-NC-6124-A3-mz-13	14996	7485	--	12.047	0.07180	0.4992	0.0024	0.8117	2606	6	2608	6	2610	10	0
15-NC-6124-A3-mz-2	10418	5225	--	12.134	0.06924	0.5015	0.0023	0.7939	2611	6	2615	5	2620	10	0
15-NC-6124-A3-mz-3	10767	5426	--	12.268	0.06283	0.5040	0.0021	0.8003	2621	5	2625	5	2631	9	0
15-NC-6124-A3-mz-24	13196	6681	--	12.328	0.10151	0.5063	0.0034	0.8177	2621	8	2630	8	2641	15	-1
15-NC-6124-A3-mz-18	14361	7186	--	12.191	0.08257	0.5004	0.0026	0.7793	2622	7	2619	6	2615	11	0
15-NC-6124-A3-mz-27	13140	6805	--	12.613	0.11380	0.5179	0.0039	0.8262	2622	8	2651	8	2690	16	-3
15-NC-6124-A3-mz-12	10561	5330	--	12.302	0.06618	0.5047	0.0022	0.7954	2623	5	2628	5	2634	9	-1
15-NC-6124-A3-mz-22	11340	5701	--	12.273	0.08563	0.5028	0.0028	0.7946	2625	7	2626	7	2626	12	0
15-NC-6124-A3-mz-14	11403	5756	--	12.341	0.07417	0.5048	0.0024	0.7771	2628	6	2631	6	2634	10	0
15-NC-6124-A3-mz-10	8512	4319	--	12.423	0.06720	0.5074	0.0021	0.7723	2630	6	2637	5	2645	9	-1
15-NC-6124-A3-mz-25	12584	6308	--	12.269	0.10807	0.5013	0.0038	0.8496	2630	8	2625	8	2619	16	0
15-NC-6124-A3-mz-16	11816	5984	--	12.403	0.07546	0.5064	0.0025	0.8002	2631	6	2635	6	2641	11	0
15-NC-6124-A3-mz-17	12681	6360	--	12.312	0.08303	0.5015	0.0027	0.8041	2635	7	2628	6	2620	12	1
15-NC-6124-A3-mz-9	8904	4469	--	12.350	0.06890	0.5019	0.0021	0.7655	2639	6	2631	5	2622	9	1
15-NC-6124-A3-mz-21	6844	3437	--	12.498	0.09197	0.5022	0.0029	0.7952	2657	7	2643	7	2623	13	2
15-NC-6124-A3-mz-11	6703	3441	--	12.782	0.06960	0.5134	0.0022	0.7887	2658	6	2664	5	2671	9	-1
15-NC-6124-A3-mz-7	3355	1690	--	12.626	0.07241	0.5037	0.0022	0.7586	2669	6	2652	5	2630	9	2
15-NC-6124-A3-mz-20	4192	2152	--	12.882	0.09828	0.5134	0.0031	0.7909	2671	8	2671	7	2671	13	0
15-NC-6124-A3-mz-4	2009	1017	--	12.745	0.07666	0.5064	0.0023	0.7551	2676	7	2661	6	2641	10	2
15-NC-6124-A3-mz-26	2185	1137	--	13.092	0.11524	0.5202	0.0037	0.7973	2676	9	2686	8	2700	15	-1
15-NC-6124-A3-mz-6	1845	928	--	12.699	0.08118	0.5030	0.0025	0.7814	2681	7	2658	6	2627	11	2
15-NC-6124-A3-mz-23	1796	921	--	12.956	0.11866	0.5126	0.0037	0.7892	2683	9	2676	9	2668	16	1
15-NC-6124-A3-mz-15	1930	1002	--	13.313	0.08156	0.5191	0.0023	0.7337	2707	7	2702	6	2695	10	1

Table 2: LA-ICPMS U-Pb zircon and monazite geochronology data for the Lac Joubert region.

Spot	U (ppm)	Pb^{206} (ppm)	Th/U	$^{207}Pb/^{235}U$	1 Sig	$^{206}Pb/^{238}U$	1 Sig	Err. Correl.	$^{207}Pb/^{206}Pb$ Age (Ma)	1 Sig	$^{207}Pb/^{235}U$ Age (Ma)	1 Sig	$^{206}Pb/^{238}U$ Age (Ma)	1 Sig	Disc. (%)
15-NC-6050-B	**Monazite**														
15-NC-6050-B-m-12.2r	25945	13370	--	12.635	0.11393	0.5153	0.0037	0.8062	2633	9	2653	8	2679	16	-2
15-NC-6050-B-m-13	17282	8994	--	12.877	0.11748	0.5204	0.0037	0.7713	2648	10	2671	9	2701	16	-2
15-NC-6050-B-m-5	9355	4867	--	12.891	0.13023	0.5202	0.0041	0.7869	2650	10	2672	10	2700	18	-2
15-NC-6050-B-m-17.2r	9673	4926	--	12.615	0.11978	0.5093	0.0039	0.8064	2650	9	2651	9	2653	17	0
15-NC-6050-B-m-3	6445	3345	--	12.867	0.10158	0.5190	0.0032	0.7741	2651	8	2670	7	2695	13	-2
15-NC-6050-B-m-1	9342	4847	--	12.876	0.10342	0.5189	0.0033	0.8010	2653	8	2671	8	2695	14	-2
15-NC-6050-B-m-2	7739	4080	--	13.103	0.09943	0.5272	0.0032	0.7894	2655	8	2687	7	2730	13	-3
15-NC-6050-B-m-4	14611	7664	--	13.056	0.10128	0.5245	0.0032	0.7833	2658	8	2684	7	2718	13	-3
15-NC-6050-B-m-9.3r	12284	6200	--	12.582	0.12570	0.5047	0.0034	0.6650	2660	12	2649	9	2634	14	1
15-NC-6050-B-m-11	19096	9974	--	13.023	0.11743	0.5223	0.0038	0.8013	2661	9	2681	9	2709	16	-2
15-NC-6050-B-m-15	15668	8039	--	12.802	0.12057	0.5131	0.0038	0.7889	2662	10	2665	9	2670	16	0
15-NC-6050-B-m-16	14519	7420	--	12.761	0.11027	0.5111	0.0035	0.7867	2663	9	2662	8	2661	15	0
15-NC-6050-B-m-17.1c	8007	4090	--	12.752	0.12660	0.5108	0.0040	0.7966	2663	10	2662	9	2660	17	0
15-NC-6050-B-m-7	11327	5840	--	12.883	0.12650	0.5156	0.0041	0.8097	2664	10	2671	9	2680	17	-1
15-NC-6050-B-m-12.1c	5292	2722	--	12.858	0.10985	0.5145	0.0035	0.7968	2664	9	2669	8	2676	15	-1
15-NC-6050-B-m-10	10184	5177	--	12.712	0.11408	0.5083	0.0035	0.7682	2666	10	2659	8	2649	15	1
15-NC-6050-B-m-6	9373	4881	--	13.162	0.13132	0.5207	0.0042	0.8117	2683	10	2691	9	2702	18	-1
15-NC-6050-B-m-9.2z	4986	2618	--	13.360	0.12799	0.5252	0.0040	0.7918	2694	10	2705	9	2721	17	-1
15-NC-6050-B-m-9.1c	6081	3087	--	12.973	0.12183	0.5077	0.0038	0.8041	2701	9	2678	9	2647	16	2
15-NC-6050-B-m-8	7829	4058	--	13.310	0.13097	0.5184	0.0041	0.8075	2709	10	2702	9	2692	17	1

Table 2: LA-ICPMS U-Pb zircon and monazite geochronology data for the Lac Joubert region.

Spot	U (ppm)	Pb^{206} (ppm)	Th/U	$^{207}Pb/^{235}U$	1 Sig	$^{206}Pb/^{238}U$	1 Sig	Err. Correl.	$^{207}Pb/^{206}Pb$ Age (Ma)	1 Sig	$^{207}Pb/^{235}U$ Age (Ma)	1 Sig	$^{206}Pb/^{238}U$ Age (Ma)	1 Sig	Disc. (%)
15-NC-6127-B	**Zircon**														
15-NC-6127-13.2Ur	1071	558	0.02	12.772	0.09910	0.5216	0.0034	0.8351	2631	7	2663	7	2706	14	-4
15-NC-6127-5.2Ur	1051	552	0.02	12.880	0.07785	0.5251	0.0023	0.7296	2633	7	2671	6	2721	10	-4
15-NC-6127-31.2Ur	1009	519	0.02	12.657	0.10228	0.5147	0.0034	0.8225	2638	8	2654	8	2677	15	-2
15-NC-6127-10Ur	860	470	0.02	13.482	0.10752	0.5471	0.0038	0.8770	2641	6	2714	8	2813	16	-8
15-NC-6127-14z	174	94	0.57	13.710	0.12237	0.5388	0.0039	0.8202	2694	8	2730	8	2779	17	-4
15-NC-6127-11zc	359	198	1.43	14.102	0.10403	0.5516	0.0031	0.7526	2702	8	2757	7	2832	13	-6
15-NC-6127-23z	1067	581	0.38	13.927	0.09878	0.5439	0.0031	0.8058	2705	7	2745	7	2800	13	-4
15-NC-6127-13.1c	273	151	0.67	14.128	0.12575	0.5513	0.0040	0.8151	2706	9	2758	8	2831	17	-6
15-NC-6127-4zc	243	128	0.84	13.582	0.09588	0.5281	0.0027	0.7322	2712	8	2721	7	2733	12	-1
15-NC-6127-3z	165	88	0.77	13.797	0.10886	0.5328	0.0033	0.7804	2723	8	2736	7	2753	14	-1
15-NC-6127-31.1c	61	31	0.79	13.318	0.12414	0.5132	0.0035	0.7242	2727	11	2702	9	2670	15	3
15-NC-6127-5.1c	25	14	0.79	14.574	0.17756	0.5466	0.0046	0.6879	2771	14	2788	12	2811	19	-2
15-NC-6127-26.1c	47	27	0.36	15.046	0.15914	0.5599	0.0048	0.8169	2784	10	2818	10	2866	20	-4
15-NC-6127-7s	233	124	0.89	14.391	0.12197	0.5326	0.0038	0.8336	2793	8	2776	8	2752	16	2
15-NC-6127-24z	130	73	0.66	15.897	0.12267	0.5573	0.0034	0.7799	2881	8	2871	7	2856	14	1
15-NC-6127-20c	179	101	0.68	16.212	0.12463	0.5660	0.0035	0.7965	2888	8	2889	7	2891	14	0
15-NC-6127-9z	153	90	0.58	17.197	0.17090	0.5862	0.0048	0.8160	2927	9	2946	10	2974	19	-2
15-NC-6127-B	**Monazite**														
15-NC-6127-B-m-1	5813	3089	--	12.951	0.13280	0.5314	0.0044	0.8026	2623	10	2676	10	2747	18	-6
15-NC-6127-B-m-2.1c	7905	4095	--	12.741	0.11580	0.5180	0.0038	0.7997	2638	9	2661	9	2691	16	-2
15-NC-6127-B-m-2.2r	5222	2706	--	12.691	0.11669	0.5182	0.0039	0.8263	2631	9	2657	9	2691	17	-3
15-NC-6127-B-m-3	5039	2626	--	12.747	0.10757	0.5211	0.0035	0.7994	2629	8	2661	8	2704	15	-4
15-NC-6127-B-m-4	9236	4723	--	12.400	0.10704	0.5114	0.0035	0.8020	2614	9	2635	8	2663	15	-2
15-NC-6127-B-m-5	4718	2464	--	12.708	0.09910	0.5222	0.0033	0.8062	2620	8	2658	7	2709	14	-4
15-NC-6127-B-m-6	5122	2644	--	12.594	0.15061	0.5161	0.0050	0.8172	2625	11	2650	11	2683	21	-3
15-NC-6127-B-m-7	6057	3133	--	12.659	0.12424	0.5173	0.0041	0.8156	2630	9	2655	9	2688	18	-3
15-NC-6127-B-m-8	4967	2602	--	12.802	0.12404	0.5238	0.0041	0.8004	2627	10	2665	9	2715	17	-4
15-NC-6127-B-m-9	13573	7073	--	12.522	0.11624	0.5211	0.0040	0.8197	2599	9	2644	9	2704	17	-5
15-NC-6127-B-m-10.1c	7896	4012	--	12.452	0.10868	0.5080	0.0036	0.8148	2632	8	2639	8	2648	15	-1
15-NC-6127-B-m-10.2r	5057	2653	--	12.856	0.11268	0.5246	0.0037	0.7955	2632	9	2669	8	2719	15	-4
15-NC-6127-B-m-11	5733	2959	--	12.574	0.11826	0.5162	0.0039	0.8118	2622	9	2648	9	2683	17	-3